



No nebular magnetization in the Allende CV carbonaceous chondrite

R.R. Fu^{*}, E.A. Lima, B.P. Weiss

Department of Earth, Atmospheric and Planetary Sciences, Massachusetts Institute of Technology, Cambridge, MA, USA



ARTICLE INFO

Article history:

Received 20 March 2014

Received in revised form 10 July 2014

Accepted 12 July 2014

Available online xxxx

Editor: C. Sotin

Keywords:

paleomagnetism
meteoritics
planetary accretion
chondrules
planetary dynamos
CV chondrites

ABSTRACT

Magnetic fields in the solar nebula may have played a central role in mass and angular momentum transport in the protosolar disk and facilitated the accretion of the first planetesimals. Thought to be key evidence for this hypothesis is the high unblocking-temperature, randomly oriented magnetization in chondrules in the Allende CV carbonaceous chondrite. However, it has recently been realized that most of the ferromagnetic minerals in Allende are products of secondary processes on the parent planetesimal. Here we reevaluate the pre-accretional magnetism hypothesis for Allende using new paleomagnetic analyses of chondrules including the first measurements of mutually oriented subsamples from within individual chondrules. We confirm that Allende chondrules carry a high-temperature component of magnetization that is randomly oriented among chondrules. However, we find that subsamples of individual chondrules are also non-unidirectionally magnetized. Therefore, the high-temperature magnetization in Allende chondrules is not a record of nebular magnetic fields and is instead best explained by remagnetization during metasomatism in a $<8 \mu\text{T}$ magnetic field. This low field intensity suggests that any core dynamo on the CV parent body decayed before the end of metasomatism, likely <40 My after the formation of calcium aluminum-rich inclusions (CAIs). Despite widespread practice, the magnetization in Allende should not be used to constrain magnetic fields in the protosolar nebula.

© 2014 Elsevier B.V. All rights reserved.

1. Introduction

During the first several million years of planet formation, dust in the solar nebula accreted to form 100 to 1000 km-scale planetesimals (Chambers, 2004). Theoretical models strongly suggest that magnetic fields played a critical role in the dynamics of the nebular gas and the evolution of solid particles. In particular, large-scale mass and angular momentum transfer in the nebula may have relied on magnetocentrifugal winds and/or turbulence generated by the magnetorotational instability (MRI) (Bai and Stone, 2013; Balbus, 2003). Magnetically-induced turbulence may have also facilitated mutual collisions and local concentration of solid matter, thereby allowing for the accretion of solid bodies (e.g., Cuzzi and Hogan, 2003; Johansen et al., 2007).

The first known macroscopic solids to form in the solar nebula were chondrules and CAIs, millimeter-sized inclusions now found in chondritic meteorites. Chondrules are igneous spherules that melted and cooled quickly in the solar nebula, while CAIs are nebular condensation products often subjected to subsequent reheating (MacPherson, 2007). Because they were heated and cooled

in the solar nebula, these objects may have recorded the nebular magnetic field. Therefore, paleomagnetic studies of chondrules and CAIs can potentially provide direct constraints on the strength of nebular magnetic fields and their role in solar system formation. Fields in the midplanes of the terrestrial planet-forming region in protoplanetary disks are currently inaccessible to astronomical measurements (Crutcher, 2012).

Paleomagnetism of chondrite inclusions such as chondrules and CAIs may also have important implications for the setting and mechanism of chondrule formation (Desch et al., 2012). Chondrule formation hypotheses often predict very different magnetic field environments (Desch and Connolly, 2002; McNally et al., 2013). Knowledge of the magnetic field intensity in the chondrule-forming environment would therefore provide new constraints on this enigmatic process.

However, paleomagnetic studies of primitive inclusions face the challenge that chondrules and CAIs in all meteorites have been subject to a combination of secondary alteration and metamorphic reheating after their accretion onto their parent body. These processes may have compromised any pre-accretional natural remanent magnetization (NRM). Furthermore, many meteorite samples experienced remagnetization in strong artificial magnetic fields on Earth following their collection. Such strong fields, if not properly identified and removed, can lead to misinterpretation and severe

^{*} Corresponding author. Tel.: +1 510 304 9435.

E-mail address: rogerfu@mit.edu (R.R. Fu).

overestimates of ancient magnetic field strengths (Weiss et al., 2010).

Paleomagnetic tests can aid in distinguishing between pre-accretional and post-accretional NRM in chondrites. In the *conglomerate test*, mutually random magnetization directions in chondrules and other inclusions provide evidence for magnetization predating the final assembly of the rock. This is because if the chondrules were completely remagnetized in a spatially uniform field following accretion, they should be magnetized in the same direction within a given meteorite. A second, *unidirectionality test* examines the direction of magnetization in subsamples of individual chondrules and CAIs. A pre-accretional thermoremanent magnetization (TRM) is expected to be unidirectional across subsamples. Both paleomagnetic tests require analysis of mutually oriented samples.

The Allende CV carbonaceous chondrite is probably the most extensively analyzed chondrite using paleomagnetic methods. Measurements of individual, unoriented chondrules (Acton et al., 2007; Emmerton et al., 2011; Lanoix et al., 1978) have inferred magnetic field paleointensities of between 10 and 1600 μT . However, these studies could not establish a pre-accretional origin for the magnetization or rule out artificial isothermal remanent magnetization (IRM) contamination. The latter almost certainly accounts for the paleointensity values $>200 \mu\text{T}$ (Cisowski, 1987; Wasilewski, 1981). Neglecting those affected by IRM, bulk Allende samples and some isolated chondrules carry a strong unidirectional overprint that unblocked below $\sim 300^\circ\text{C}$ acquired on the CV parent body (Carporzen et al., 2011; Nagata, 1979a; Sugiura and Strangway, 1985). Carporzen et al. (2011) interpreted this post-accretional magnetization, which they called the middle temperature (MT) component, as evidence for a past magnetic core dynamo on the CV parent body, implying that this body underwent igneous differentiation while preserving a relatively unheated chondritic crust.

Nevertheless, paleomagnetic studies by Sugiura et al. (1979) and Sugiura and Strangway (1985) showed that, after removal of the low temperature overprint at $\sim 300^\circ\text{C}$, individual, mutually-oriented chondrules in Allende had widely scattered magnetization directions that pass the paleomagnetic conglomerate test at the 95% significance level (Watson, 1956). Sugiura and Strangway (1985) concluded that this non-unidirectional component is a pre-accretional TRM acquired in a nebular magnetic field.

However, a major source of subsequent confusion has been that no paleointensities were reported for this non-unidirectional HT component. As a result, many later studies have mistakenly cited paleointensities derived for the other magnetization components in Allende as constraints on nebular fields. In particular, many theoretical studies (e.g., Levy and Araki, 1989; Stepinski, 1992; Rozyczka et al., 1996; Shu et al., 1996; Nübold and Glassmeier, 2000; Desch and Connolly, 2002; Johansen, 2009) have cited the $\sim 100 \mu\text{T}$ paleointensity values derived from unoriented chondrules or bulk samples (which should be dominated by the post-accretional MT overprint) or even the high paleointensities of 100–1600 μT from a set of unoriented chondrules likely contaminated by IRMs on Earth (Wasilewski, 1981).

Adding to the uncertainty, the paleomagnetic conglomerate test alone, as performed by Sugiura and Strangway (1985), is in fact insufficient for establishing the pre-accretional origin of the HT chondrule magnetization. Post-accretional recrystallization of magnetic phases in a near-zero magnetic field can also produce randomized magnetization directions (Uehara et al., 2011), potentially leading to a false-positive conglomerate test. In fact, the weak intensity of the HT magnetization and its non-origin trending behavior during higher temperature thermal demagnetization are all characteristics of such null field remanence (see Section 4.1).

Here we report new paleomagnetic analyses on mutually-oriented Allende chondrules and subsamples of individual chondrules with the goal of determining whether the HT component in Allende chondrules is in fact pre-accretional. We find that, although the HT magnetizations of individual chondrules pass the conglomerate test, *subsamples* of individual chondrules also have statistically random magnetization directions, thereby failing the unidirectionality test. Coupled with petrographic observations and modeling of TRM acquisition in the solar nebula, we argue that all observed magnetization components in Allende chondrules are post-accretional. Finally, we discuss the implications of these results for the CV parent body core dynamo hypothesis and the lifetime of such a dynamo.

2. Samples and methods

We performed two kinds of paleomagnetic measurements. The bulk of our analyses employed classic moment magnetometry using a 2G Enterprises Superconducting Rock Magnetometer (2G SRM) 755 at the MIT Paleomagnetism Laboratory. These were supplemented with magnetic field maps acquired with the MIT SQUID Microscope (Weiss et al., 2007).

Samples analyzed using the 2G SRM were extracted from a slab of Allende provided by the American Museum of Natural History called AMNH5056, which is a $\sim 10 \times 10 \times 0.8 \text{ cm}$ piece previously studied by Carporzen et al. (2011). All samples taken from AMNH5056 are mutually oriented with respect to samples in Carporzen et al. (2011).

Carporzen et al. (2011) conducted a fusion crust baked contact test (Nagata, 1979b; Weiss et al., 2010) on AMNH5056 and showed that the fusion crust, which was melted during atmospheric entry, carries magnetization distinct from that in samples taken $\geq 1 \text{ mm}$ in the interior. This systematic change in magnetization direction and intensity indicates that AMNH5056 escaped significant remagnetization after its arrival on Earth and that the interior magnetization is extraterrestrial in origin. Because AMNH5056 had been stored in the magnetically shielded room at the MIT Paleomagnetism Laboratory (DC field $< 150 \text{ nT}$) since the experiments in Carporzen et al. (2011), their demonstration of extraterrestrial magnetization in AMNH5056 applies to our samples extracted from this parent piece.

We used nonmagnetic dental tools to extract twenty-one chondrules and six matrix-rich samples from thin (0.5–1.0 mm) slices of Allende cut using a diamond wire saw. Because the Allende matrix is on average 2–4 times more magnetic per unit mass than typical chondrules and CAIs (Table S1; Emmerton et al., 2011; Nagata and Funaki, 1983), we carefully removed all visible traces of matrix material adhered to chondrules. When possible, we subsampled individual chondrules using either a diamond wire saw or dental tools. Seven of the twenty-one chondrules were partitioned into at least two mutually oriented pieces. All chondrule and matrix samples were mutually oriented to better than 5° accuracy. Samples were numbered before extraction, resulting in unused numbers among the successfully extracted and measured samples. We mounted all samples on GE 124 quartz disks with cyanoacrylate or non-magnetic silver paste (SPI Silver Paste Plus). All sample mounts and adhesive had moments less than $\sim 5 \times 10^{-12} \text{ Am}^2$, which is the effective noise level of our 2G SRM measurements.

Twelve chondrule samples from six distinct chondrules and four matrix-rich samples were subjected to stepwise thermal demagnetization in air up to the point when the magnetization direction became incoherent or the sample moment spontaneously increased due to alteration of magnetic phases, which occurred at $\leq 420^\circ\text{C}$. Additionally, two matrix-rich samples and thirteen chondrule subsamples from eleven distinct chondrules were subjected to three-axis alternating field (AF) demagnetization up to 85 mT.

Samples mapped using SQUID microscopy include one 30 μm thin section from AMNH5056 and the five isolated chondrules from a second Allende slab called AMNH4889 (see Supplementary Data, SD). The thin section was prepared without any heating using cyanoacrylate and bronze saw blades. Non-magnetic alumina-based polishing agents were used during thin section preparation to minimize contamination.

The MIT SQUID Microscope acquires maps of the vertical component of the magnetic field produced by geological samples with 100–200 μm spatial resolution and ultra-high sensitivity (Fong et al., 2005; Weiss et al., 2007). We first measured the magnetic field of the AMNH5056 thin section at a sensor-to-sample distance of ~ 200 μm with a step size of 80 μm . It is usually not possible to calculate uniquely the fine-scale (<200 μm) non-unidirectional magnetization distribution from raw field measurements (Baratchart et al., 2013). Instead, we enhanced the magnetic field map using potential field techniques. Following Lima et al. (2013), we first performed a bilinear interpolation of the field map by a factor of 2 in each horizontal direction. We then downward continued the field map to obtain an effective sensor-to-sample distance of 100 μm with a step size of 40 μm . Finally, we computed the full three-component vector field using the procedure described in Lima and Weiss (2009) and used this to obtain the total field map. The thin section was subjected to stepwise three-axis AF demagnetization up to 39 mT to remove any possible low-coercivity overprints due to sample preparation. The close agreement between NRM directions recovered from the 2G SRM samples and the thin section confirms the lack of contamination (see Section 3.2). Finally, to characterize the magnetic mineralogy of Allende material, we performed electron microprobe analyses on two isolated chondrules and one matrix-rich sample using a JEOL-JXA-8200 Superprobe in the MIT Experimental Petrology Laboratory.

3. Results

3.1. The Allende matrix carries a strong, unidirectional magnetization

Isolated matrix-rich samples carry a strong unidirectional NRM oriented in the same direction as that of the bulk samples measured by Carporzen et al. (2011) (Fig. 1A; please see online supplement for all demagnetization data). Among our samples, the matrix, which composes $\sim 40\%$ of bulk material (Weisberg et al., 2006), has an average mass-normalized NRM intensity for millimeter-sized samples that is ~ 4 times higher than that of chondrules (Tables S1 and S2). Furthermore, the NRMs of most chondrules are randomly oriented (see Section 3.2), which further reduces their combined contribution to the net magnetization of bulk material compared to the unidirectionally magnetized matrix. Therefore, matrix magnetization dominates that of bulk Allende material, explaining the similarity in NRM directions of matrix-rich and bulk samples. The highly uniform NRM intensity varies $<40\%$ among the seven matrix samples.

Thermal demagnetization of four matrix-rich samples reveals two unidirectional components of magnetization (Fig. 2A) similar to those observed by Carporzen et al. (2011) for bulk samples. A weak ($\sim 5 \times 10^{-5}$ $\text{Am}^2 \text{kg}^{-1}$) low temperature (LT) component is blocked between room temperature and 100 $^{\circ}\text{C}$. A stronger ($\sim 2 \times 10^{-4}$ $\text{Am}^2 \text{kg}^{-1}$) MT component is blocked between 100 $^{\circ}\text{C}$ and 260–280 $^{\circ}\text{C}$. Finally, we observe a much weaker ($\sim 1 \times 10^{-5}$ $\text{Am}^2 \text{kg}^{-1}$), non-unidirectional HT magnetization in two of the four matrix-rich samples. The HT magnetization does not decay to the origin for most subsamples during thermal demagnetization and remains stable in direction until ~ 325 –420 $^{\circ}\text{C}$, at which point it loses directional coherence. Such unstable demagnetization behavior at higher temperatures is likely due to chemical alteration of magnetic phases, as significant alteration during heating

in air has been observed for Allende material at as low as 320 $^{\circ}\text{C}$ (Carporzen et al., 2011). To test this hypothesis, we conducted stepwise heating on matrix-rich sample MC while performing IRM acquisition after each heating step. We observed that the saturation IRM intensity of the sample increased by a factor of 1.7 between 360 $^{\circ}\text{C}$ and 390 $^{\circ}\text{C}$, indicating the alteration of magnetic phases. Therefore, 325–420 $^{\circ}\text{C}$ represents a lower bound on the true upper unblocking temperature of the HT magnetization.

The MT component direction is indistinguishable from those observed for bulk samples from AMNH5056 (Fig. 1D) (Carporzen et al., 2011). The small offset between our mean LT component direction and that of Carporzen et al. (2011) is likely due to small (5°) errors in the mutual orientations between our samples and the ones used in Carporzen et al. (2011). Likewise, the non-unidirectional HT component observed in our matrix samples was also previously observed in bulk samples from AMNH5056. During AF demagnetization, two matrix samples exhibited single-component, unidirectional magnetization whose intensity decayed by only 38–42% by 85 mT (Fig. 3), again consistent with previous measurements of bulk samples (Carporzen et al., 2011).

3.2. Isolated chondrules carry mutually and internally non-unidirectional magnetization

In contrast to the uniform magnetization of matrix samples, NRM intensities for chondrule samples vary across two orders of magnitude (Table S2). We assign all Allende chondrules to one of two classes with systematically different magnetic properties (Table 1). Class A chondrules carry the same strong MT component of magnetization as in matrix material. As with the matrix-rich samples the MT component in class A chondrules is unblocked between ~ 100 $^{\circ}\text{C}$ and 274–286 $^{\circ}\text{C}$ (Fig. 1D; Fig. 2B) and has intensities of 1.1×10^{-4} $\text{Am}^2 \text{kg}^{-1}$ or higher. In contrast, class B chondrules do not carry this overprint and therefore have much lower NRM intensity (Fig. 2C; Table S2).

Due to the high intensity of their MT overprint, the NRM directions of class A chondrules cluster around the mean MT component direction similar to bulk and matrix-rich samples (Fig. 1B). Upon the demagnetization of the MT component, matrix and class A chondrule samples have lost $\sim 90\%$ of their initial NRM intensities (Fig. 4). In contrast, because class B chondrules do not carry the MT overprint, their magnetic moments exhibit limited decay below 300 $^{\circ}\text{C}$.

Seven out of thirteen chondrule samples from both classes A and B subjected to thermal demagnetization carry a weak ($\sim 3 \times 10^{-5}$ $\text{Am}^2 \text{kg}^{-1}$) LT component unblocked below 110 $^{\circ}\text{C}$ and nearly parallel to the LT component of matrix samples. After the removal of any LT and MT overprints at or below 280 $^{\circ}\text{C}$, all chondrules carry an HT magnetization. As with the HT magnetization in matrix-rich samples, the HT magnetization in chondrules exhibits random directions (Figs. 1D and 2D), and is consistent with the HT chondrule remanence described in Sugiura and Strangway (1985). This HT magnetization is directionally stable until at least 314–420 $^{\circ}\text{C}$, at which point mineralogical alteration occurs.

Class A and B chondrules also show systematically different behaviors during AF demagnetization. The NRMs of class A chondrules remain directionally stable during AF demagnetization up to 85 mT, which is similar to the behavior of matrix-rich samples (Fig. 3A, B). In contrast, class B chondrule samples exhibit highly unstable NRM during AF demagnetization at all AF levels (Fig. 3C). We therefore identify class A and class B chondrules with the “AF stable” and “AF unstable” chondrules described by Wasilewski and Saralker (1981), respectively. As further support of this correspondence, Wasilewski and Saralker (1981) reported that 14 out of 20 chondrules are “AF unstable”, which is similar to our proportion of class B chondrules (17 out of 21).

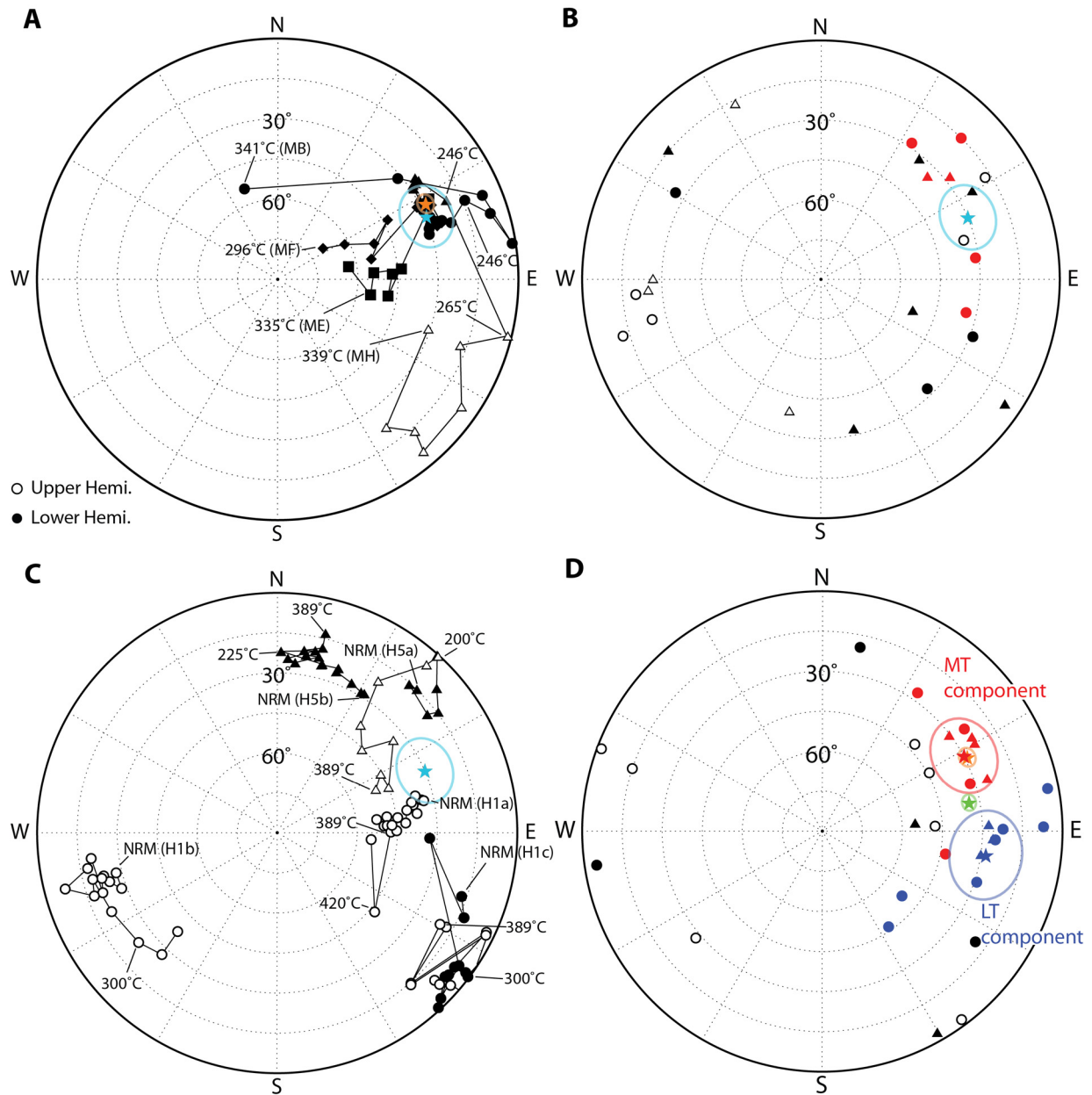


Fig. 1. NRM directions in Allende chondrules and matrix-rich samples. Shown are equal area stereographic projections with solid (open) symbols representing lower (upper) hemisphere. (A) Thermal demagnetization of four isolated Allende matrix-rich samples (MB, ME, MF, and MH). Light blue star and circle correspond to the MT component direction and associated 95% confidence interval of matrix-rich samples from this study. Orange star and circle indicate the average MT component direction and associated 95% confidence interval for bulk Allende samples measured by Carporzen et al. (2011). Each subsample is assigned a different symbol (i.e., circle, square, diamond, and triangle). NRM directions for all four subsamples lie within the 95% confidence interval of the mean (i.e., within light blue circle). Selected demagnetization temperatures are labeled. (B) NRM directions of all chondrule samples. Triangles denote samples subjected to AF demagnetization and circles denote samples subjected to thermal demagnetization. Red symbols correspond to class A chondrule samples (which have strong MT overprints and are stable upon AF demagnetization), and black symbols correspond to class B chondrule samples (which have no MT overprint and are unstable upon AF demagnetization). As in panel (A), light blue star and circle correspond to MT component direction of matrix samples from this study. Note the clustering of class A chondrule sample NRM directions around the matrix MT component direction. (C) Thermal demagnetization of subsamples from a class A (H2; triangles) and a class B (H1; circles) chondrule. As in panel (A), light blue star and circle correspond to MT component direction of matrix samples from this study. Selected demagnetization temperatures are labeled. (D) Directions of LT, MT, and HT magnetization components obtained using principal components analysis. Shown are the LT (blue), MT (red), and HT (black) magnetization directions from all thermally demagnetized chondrule (circles) and matrix (triangle) samples. Blue and red stars and ellipses indicate the average directions and 95% confidence intervals of the LT and MT components in chondrules from this study while the green and orange stars and ellipses correspond to the LT and MT components in bulk samples from Carporzen et al. (2011). Note the non-unidirectionality of the HT component directions.

Importantly, optical microscopy suggests that the major ferro-magnetic phases in “AF unstable” (class B) chondrules are sulfides, metal, and magnetite while those in “AF stable” (class A) chondrules are predominantly just sulfides (Wasilewski and Saralker, 1981). This is consistent with other previous studies showing that the magnetic phases in Allende consist of iron sulfides, high-Ni FeNi metal (awaruite), and magnetite (Butler, 1972; Carporzen et

al., 2011; Emmerton et al., 2011; Funaki and Wasilewski, 1999; Nagata and Funaki, 1983; Wasilewski and Saralker, 1981). Our electron microprobe studies of one class A and one class B chondrule show that sulfides are indeed the dominant opaque phase in the former, occurring in both the interior and in a highly sulfidized rim. Meanwhile, awaruite is the most abundant opaque phase in the class B chondrule (Fig. 5).

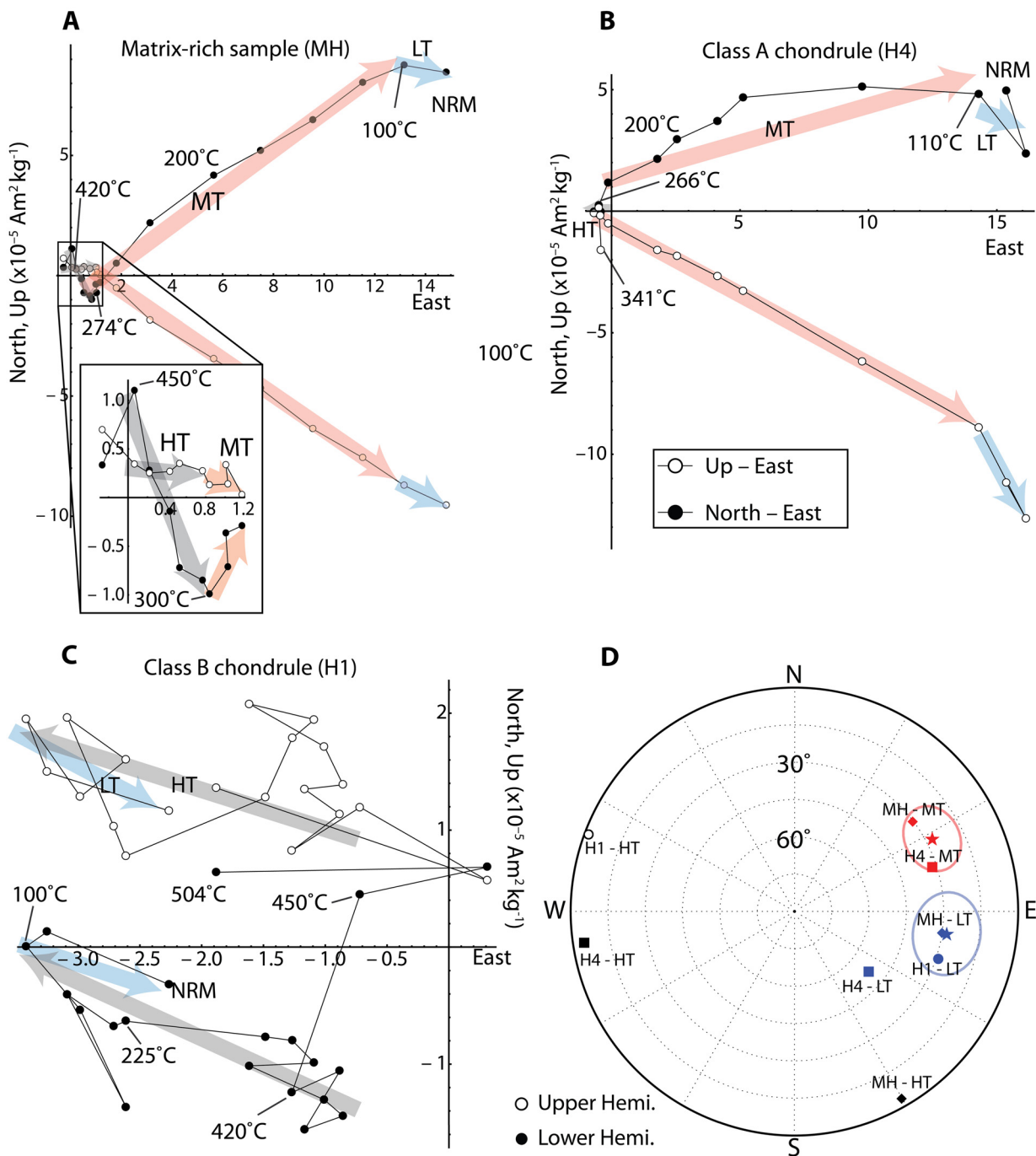


Fig. 2. Thermal demagnetization of (A) matrix-rich sample MH, (B) class A chondrule sample H4a, and (C) class B chondrule sample H1d. Open and closed circles indicate the projection of the magnetization vector onto the vertical (up-east) and horizontal (north-east) planes, respectively. Inset to panel (A) has same units as main plot. (D) Equal area stereonet showing the component directions for each sample in panels (A)–(C). All three samples carry a unidirectional low temperature (LT) and non-unidirectional high temperature (HT) component, but only the matrix-rich and class A chondrule samples carry the strong, unidirectional MT component. As in Fig. 1D, blue and red stars and ellipses indicate the average direction and 95% confidence intervals of the LT and MT components in chondrules, respectively. Open (closed) symbols denote upper (lower) hemisphere. (For interpretation of the references to color in this figure legend, the reader is referred to the web version of this article.)

The composition of the sulfides is homogeneous among the chondrules and matrix. Six quantitative wavelength dispersive spectroscopy (WDS) analyses using a $\sim 2 \mu\text{m}$ resolution beam yielded a mean composition of $\text{Fe}_{6.1}\text{Ni}_{2.8}\text{S}_{8.0}$. Assuming a low temperature formation significantly below 400°C (Carpözen et al., 2011), this composition corresponds to an equilibrium assemblage consisting of troilite, pentlandite, and hexagonal pyrrhotite (Vaughan and Craig, 1978), the last of which is ferromagnetic and may account for the rapid decay in the moment of a saturation IRM in our samples below 270°C upon thermal demagnetization

(see SD and Fig. S3). Further, pentlandite is commonly observed in other oxidized CV chondrites where it may be intergrown with pyrrhotite at the $<2 \mu\text{m}$ scale (Brearley and Krot, 2012; Krot et al., 1997, 1998a, 1998b).

We note that the dichotomy between class A and B chondrules is not clearly related to the FeO content (i.e., type I and type II chondrules) or the textural classification. Both class A and B chondrules subjected to electron microprobe analyses (Fig. 5) are type I porphyritic olivine chondrules, which are the most common classification of chondrules in Allende (McSween, 1977).

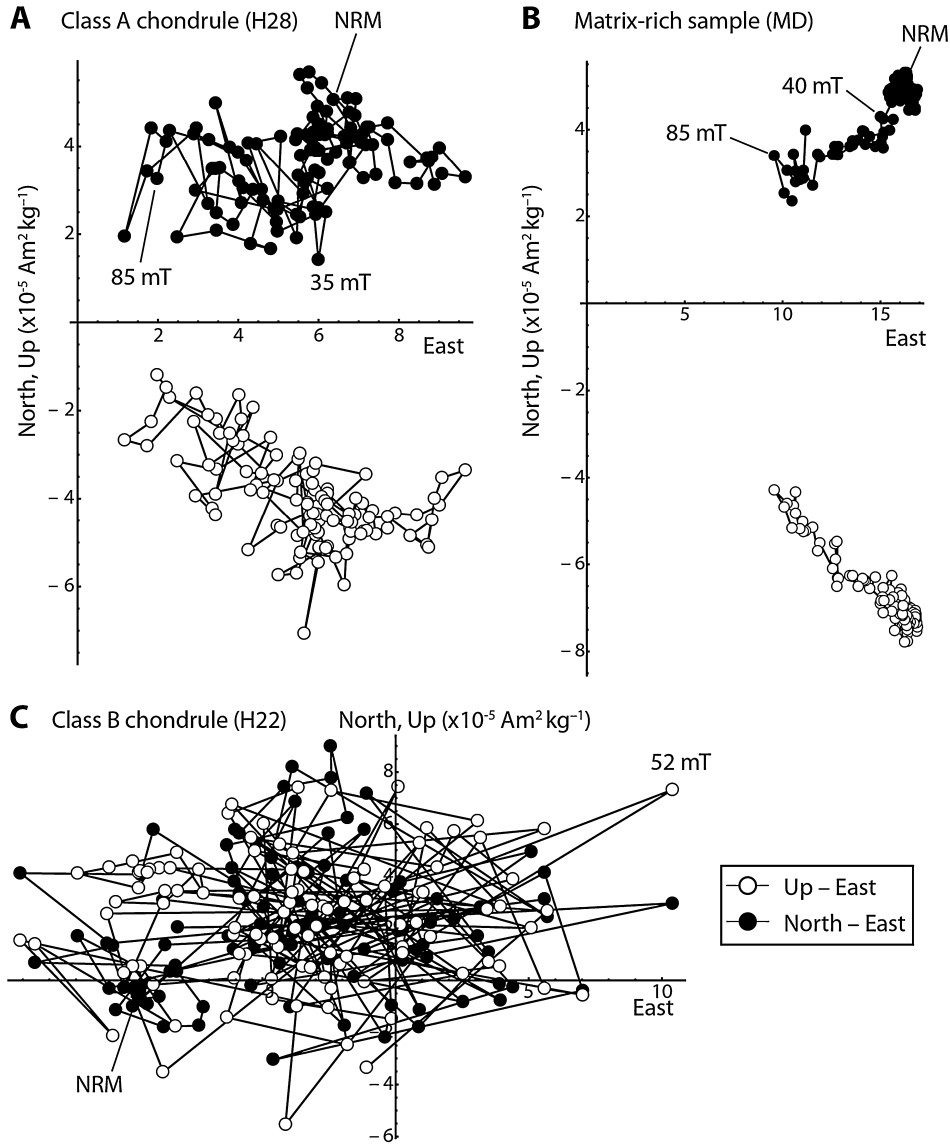


Fig. 3. AF demagnetization of Allende chondrules and matrix-rich samples. Open and closed circles indicate the projection of the magnetization vector onto the vertical (up-east) and horizontal (north-east) planes, respectively. (A) Class A chondrule H28. (B) Matrix-rich sample MD. (C) Class B chondrule H22. Note the dramatic difference in stability of the class A (panel A) and class B (panel C) chondrules.

Table 1
Summary of characteristics of class A and class B chondrules.

Class A chondrules	Class B chondrules
Carry MT component of magnetization also found in all matrix samples	Lack the MT component of magnetization
NRM directions close to the MT overprint direction	Random NRM directions
NRM intensities between 2.0 and $21.6 \times 10^{-5} \text{ Am}^2 \text{ kg}^{-1}$	NRM intensities between 0.2 and $10.4 \times 10^{-5} \text{ Am}^2 \text{ kg}^{-1}$
Subsamples of single chondrules carry unidirectional magnetization below $\sim 280^\circ\text{C}$ and non-unidirectional magnetization above	Subsamples of single chondrules carry stable, non-unidirectional magnetization between room temperature and $\sim 400^\circ\text{C}$
Stable, unidirectional magnetization upon AF demagnetization	Unstable magnetization upon AF demagnetization
Higher abundance of FeNi sulfides relative to awaruite	Higher abundance of awaruite relative to FeNi sulfides

The differences between class A and B chondrules cannot be explained by the retention of contaminating matrix material on class A chondrules. The mass-normalized magnitude of the MT component in class A chondrules is $5\text{--}18 \times 10^{-5} \text{ Am}^2 \text{ kg}^{-1}$ (Fig. 2). Given that class B chondrule materials carry no MT component and that the MT component in matrix samples is $\sim 20 \times 10^{-5} \text{ Am}^2 \text{ kg}^{-1}$, class A chondrule samples, if they are in fact a mixture of class B chondrule material and contaminating matrix, must consist of between 25 and 90 wt% matrix material

to produce the observed MT component intensities. Such extensive contamination would be readily observed.

The directions of the HT magnetization in subsamples of individual chondrules are randomly oriented (Fig. 1C). In the case of chondrule H1, which is the only chondrule that yielded more than two subsamples, subsample HT directions are statistically non-unidirectional ($P = 0.77$, where P is the probability that four random unit vectors shows greater unidirectionality; Watson, 1956). In contrast, the MT component in four total subsamples from two class A chondrule is unidirectional ($P = 0.0015$).

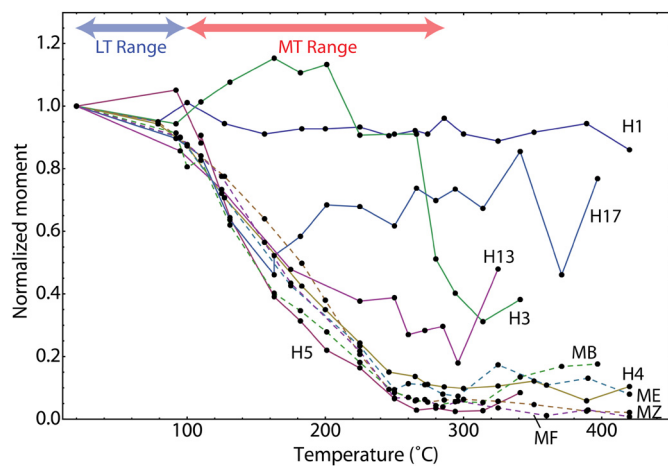


Fig. 4. Normalized moments of chondrule and matrix-rich samples during thermal demagnetization. Solid and dashed curves represent chondrules and matrix-rich material, respectively. Demagnetization was halted when samples no longer exhibited directional stability or when sample moments increased dramatically. Chondrules H4 and H5 are of class A while H1, H3, H13, and H17 are of class B.

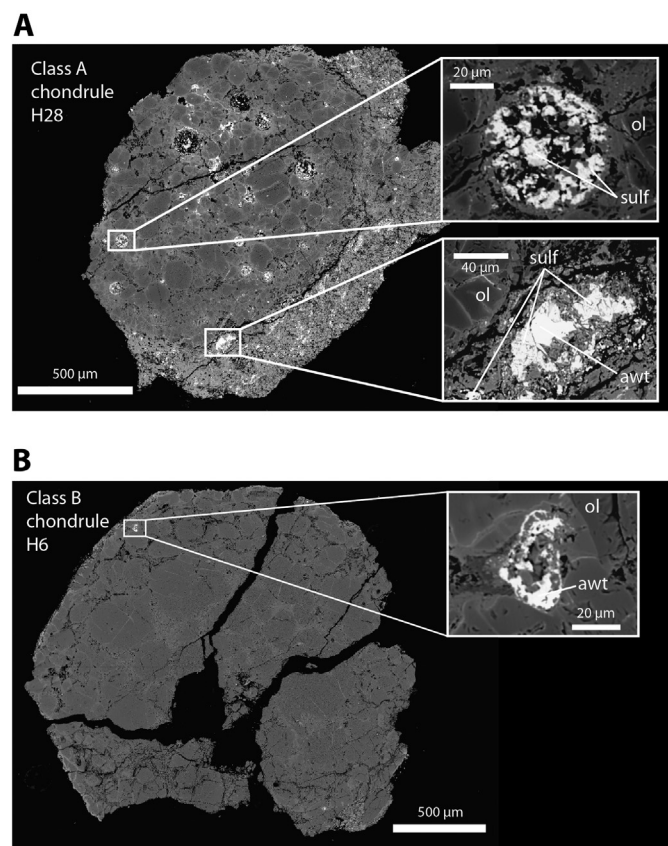


Fig. 5. Backscatter scanning electron microscopy image of (A) a class A chondrule H28 and (B) a class B chondrule H6. Insets show the composition of opaque phases in each chondrule. Abbreviations “sulf”, “awt”, and “ol” refer to FeNi sulfides, awaruite, and olivine, respectively. The higher relative abundance of sulfides in class A chondrules and of awaruite in class B chondrules is consistent with optical microscopy observations and coercivity spectra Curie temperatures (Wasilewski and Saralker, 1981).

SQUID microscopy of the Allende thin section confirms and extends our conclusion that class B chondrules have non-unidirectional magnetization (Fig. 6). To quantitatively test chondrule non-unidirectionality, we solved for the unidirectional magnetization model that best fits the magnetic field above a single chondrule in the thin section and evaluated whether such a model is

physically plausible (Fig. 6D–H). The greater abundance of awaruite compared to FeNi sulfides in the chondrule interior, observed via reflected light optical microscopy, suggests that this is a class B chondrule. We applied a spatial window to taper off contributions from adjacent sources outside of the chondrule. Following Weiss et al. (2007), we then computed the best fit magnetization intensity distribution in the chondrule for 600 uniformly distributed assumed magnetization directions. The peak magnitude of residuals for the best-fit direction is ~ 100 nT, which is 10^2 times the expected noise limit, meaning that a unidirectional solution can be rejected. Additional strong evidence for non-unidirectional magnetization is that this computed best-fit magnetization solution is nonphysical: it exhibits strong streaking, which is inconsistent with the expected distribution of ferromagnetic minerals (Fig. 6F). Thin section SQUID microscopy therefore supports the conclusion from 2G SRM measurements that class B chondrules are not unidirectionally magnetized. Although AF demagnetization of the thin section to 39 mT may have altered the magnetization, the MT component in class A chondrules and matrix material is still directionally stable at this AF level. Therefore, the non-unidirectional chondrule magnetization mapped using SQUID microscopy confirms that this chondrule belongs to class B and never carried the MT component.

To demonstrate that the non-unidirectional magnetization in Allende at sub-chondrule scales is consistent with the unidirectional NRM of bulk samples, we mapped the thin section using the SQUID Microscope at different sensor-to-sample distances (approximately 200 μm , 450 μm , and 750 μm ; Fig. 7A–B). We computed the upward continuation of the map taken 750 μm above the sample for three sensor-to-sample distances (1150 μm , 2300 μm , and 3450 μm ; Fig. 7C). We then used a two-step inversion procedure on each map to find its best unidirectional magnetization representation. The first step consists of computing the magnetization intensity distribution in the thin section for 200 uniformly distributed assumed magnetization directions and selecting the one that best fits the measured map. In the second step, we refined this result by computing inversions on a ~ 40 point fine grid spanning $\pm 15^\circ$ around both the inclination and declination found in the first step (Fig. 7F–G). A net moment estimate was directly obtained by integrating the best-fit unidirectional magnetization intensity distribution (Fig. 7E).

The uniform magnetization model is a poor representation of the Allende magnetization for sensor-to-sample distances smaller than 1000 μm . It becomes increasingly accurate for maps with larger sensor-to-sample distances, which show small normalized residuals and accurately reproduce the net moment measured by the 2G SRM (Fig. 7D–G). We stress that this progression toward a unidirectional behavior does not stem from a transition to the far-field, dipole-dominated regime given that the thin section has dimensions of $\sim 17 \text{ mm} \times 7 \text{ mm}$, which is much larger than the $\leq 3.45 \text{ mm}$ sensor-to-sample distance. Instead, the non-unidirectional magnetic fields produced by class B chondrules, although they are of a comparable intensity as those produced by the matrix at the 100 μm scale (Fig. 6), fall off much more rapidly with distance than the unidirectional MT component carried by the matrix and class A chondrules. Thus, Allende exhibits non-unidirectional behavior at sub-chondrule scales and unidirectional behavior at larger scales. Moreover, at such large spatial scales the magnetization direction converges to the direction measured for the strong, unidirectional MT component (Fig. 7D). This experiment demonstrates that SQUID microscopy can measure the spatial scale at which a sample is unidirectionally magnetized.

To characterize the magnetic recording limit and rock magnetic properties of Allende material, we conducted a suite of anhysteretic remanent magnetization (ARM) and IRM acquisition experiments. We imparted laboratory ARMs as an analog for TRM on

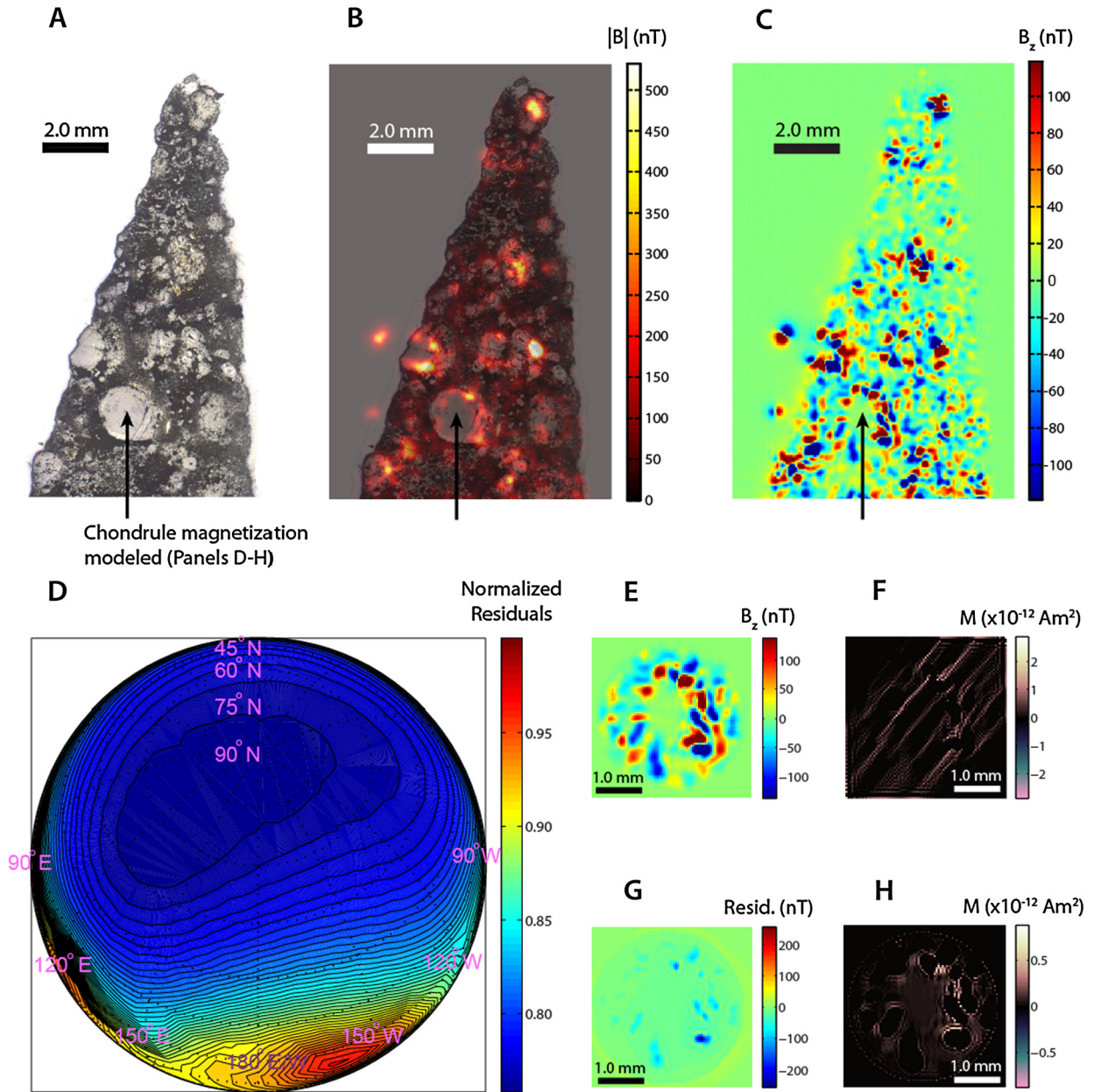


Fig. 6. SQUID Microscope measurement of a 30 μm thin section of the Allende meteorite and inversion calculations of a single chondrule. (A) Reflected light photomicrograph, (B) magnitude of the total magnetic field 100 μm above the thin section superimposed over the optical photomicrograph, and (C) vertical component of the magnetic field 100 μm above the thin section. For a single chondrule (black arrow), we fit for the three-dimensional magnetization intensity pattern assuming unidirectional magnetization oriented in 600 trial directions. The residuals (D) between the model and observed vertical fields (E) show a weak minimum (i.e., best-fit direction). However, the magnetization distribution corresponding to the best-fit direction is non-physical (F). Restricting the location of magnetization to within just the surface of the chondrule results in high residuals between the observed and model magnetic fields (G) and likewise non-physical magnetization (H). Therefore, the magnetization in this chondrule cannot be unidirectional, corroborating our results from isolated chondrule samples.

three class B chondrules to find the lowest ambient magnetic field that can be reliably recorded (see SD). Because we identified magnetization components based on the existence of a coherent magnetization direction across different samples, we define an ARM bias field level as “recordable” if the set of five ARMs acquired in the field is non-random at the 95% confidence interval (Watson, 1956) and their mean direction is consistent with the bias field direction at the 95% confidence level. By this definition, two out of the three chondrules gained a unidirectional ARM in a 2 μT bias field and one chondrule recorded a 1 μT bias field. No chondrule reliably acquired an ARM in a 0.7 μT bias field. This ~ 0.7 μT ARM recording limit implies that some class B chondrules should have acquired a 280 $^{\circ}\text{C}$ partial TRM (pTRM) in a >2 μT field given a

pTRM/ARM ratio of 0.373, which is well below the 60 μT paleointensity found for the MT component (Carpenter et al., 2011). Furthermore, the 60 μT value is likely an underestimate since the earlier authors did not account for the lack of MT magnetization in chondrules, resulting in higher intensities of laboratory pTRM, ARM, and IRM used to calculate paleointensities. Assuming that chondrules have similar mass-normalized saturation IRM intensities as matrix material and that Allende contain 40% chondrules by mass, removal of the chondrule contribution to the laboratory remanences results in a revised MT component paleointensity of ~ 100 μT .

For possible chemical remanent magnetization (CRM) in Allende chondrules (see Section 4) the ~ 0.7 μT threshold for ARM

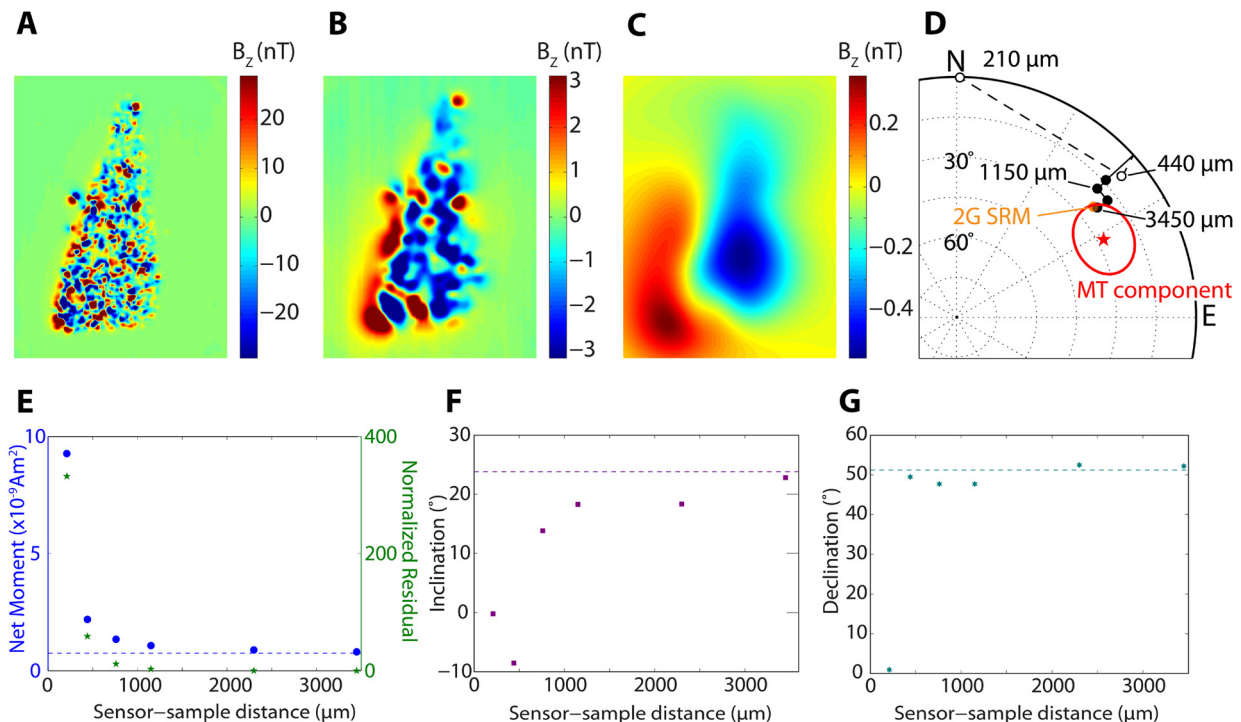


Fig. 7. Recovery of the NRM magnetization of bulk Allende material via SQUID microscopy at increasing sensor-to-sample distances. SQUID Microscope map of the vertical component of the magnetic field (A) $\sim 200 \mu\text{m}$, (B) $\sim 750 \mu\text{m}$, and (C) $\sim 3450 \mu\text{m}$ above the Allende thin section. The map in (C) was obtained by upward continuation of the magnetic data shown in (B). (D) Equal area stereonet diagram showing the best-fit magnetization direction of the thin section assuming a unidirectional magnetization model (black points). For increasing sensor-to-sample distances, the best-fit direction approaches the net magnetization direction of the sample as measured in the 2G SRM (orange) and the mean MT component direction (red star; red circle represents the 95% confidence interval). (E) Recovered net moment (blue circles) as a function of sensor-to-sample distance assuming a unidirectional magnetization distribution model. The dashed line indicates the net moment strength measured by the 2G SRM for the thin section. Also shown is the normalized residual (i.e., the norm of the difference between the model and experimental magnetic field maps divided by the norm of the experimental field map) as a function of sensor-to-sample distance (green stars). (F) Recovered inclination as a function of the sensor-to-sample distance assuming a unidirectional magnetization distribution model. The dashed line represents the inclination measured by the 2G SRM for the thin section. (G) Recovered declination as a function of the sensor-to-sample distance assuming a unidirectional magnetization distribution model. The dashed line indicates the declination of measured by the 2G SRM for the thin section. The convergence of the net magnetization recovered from the SQUID map using a unidirectional magnetization model for sensor-to-sample distances greater than $\sim 1 \text{ mm}$ confirms that the magnetization of Allende material is heterogeneous at scales less than $\sim 1 \text{ mm}$ and that the strong unidirectional MT magnetization dominates the NRM direction of bulk Allende material.

corresponds to a CRM recording limit of $< 8 \mu\text{T}$ (see SD). Furthermore, thermal demagnetization of a near-saturation IRM showed that $\sim 30\%$ of remanent magnetization in class B chondrules unblocks between room temperature and 280°C , implying that the lack of the MT component in these chondrules cannot be explained by their unblocking temperature spectrum (see SD).

Finally, progressive IRM acquisition up to 0.9 T (Fig. S2) shows that matrix material has the hardest coercivity spectrum followed by class A and then class B chondrule samples. The lower coercivities of class B chondrules are consistent with their more unstable behavior during AF demagnetization (Tikoo et al., 2012). FeNi metals, including awaruite, are typically found in the multidomain state and exhibit low coercivities (Gattacceca et al., 2014; Weiss et al., 2010). The lower coercivities of class B chondrules therefore provide further evidence that they contain a higher ratio of awaruite to pyrrhotite compared to class A chondrules and matrix material.

4. Discussion

4.1. The non-unidirectional HT magnetization is most likely a parent body chemical remanent magnetization (CRM)

Earlier studies have documented randomly oriented HT magnetization among whole Allende chondrules and used this observation to argue for a pre-accretional TRM origin (Sugiura et al., 1979, 1985). However, our measurement of non-unidirectional HT

magnetization among subsamples of single chondrules places further strong constraints on its origin. A non-unidirectional TRM in single chondrules requires that each sector of the chondrule cooled across the $> 300^\circ\text{C}$ HT blocking temperature range independently. However, the small size of chondrules implies that they cannot sustain large internal temperature contrasts for more than $\sim 2 \text{ s}$ while chondrules cooled across their blocking temperature spectrum over much longer timescales (see SD). Therefore, temperatures in a single chondrule would have homogenized before any one sector could have acquired a TRM in a unique direction; the HT magnetization cannot be a pre-accretional TRM. The HT magnetization is also not a post-accretional TRM because no heat source is likely to result in temperature contrasts of $> 300^\circ\text{C}$ at such fine scale. Impact heating, if it had a significant effect on Allende, is predicted to result in the preferential heating of the matrix instead of chondrules (Muxworthy et al., 2011).

We consider a CRM or thermochemical remanent magnetization (TCRM) origin for the HT magnetization. As described above, magnetic phases in Allende consist of iron sulfides, magnetite, and high-Ni FeNi metal (awaruite). All of these phases likely formed due to sulfidization and oxidation of primary low-Ni FeNi metal (Brearley and Krot, 2012; Haggerty and McMahon, 1979; Krot et al., 1998a). Sulfides in Allende, which include ferromagnetic pyrrhotite, show higher S excess compared to those of less altered CV chondrites such as Vigarano, suggesting an origin due to low temperature sulfidization of FeNi metal and Fe-rich sulfide phases such as troilite (Krot et al., 1998a). The oxygen isotopic

composition of Allende magnetite is distinct from that of primary olivine, indicating a secondary origin (Choi et al., 1997). The Ni-rich composition observed for FeNi metal in Allende (~70 wt% Ni) is consistent with formation due to Fe-removal in a secondary oxidation event (Haggerty and McMahon, 1979) and is broadly consistent with an observed 600–610 °C Curie point reported in previous Allende rock magnetic studies (Butler, 1972; Nagata and Funaki, 1983; Wasilewski and Saralker, 1981), which corresponds to a composition of 61–64 atomic percent (at%) Ni (Swartzendruber et al., 1991). In contrast, the primary low-Ni FeNi metal found in less altered CV chondrites (e.g., Leoville) has a nickel content of ~5 at% (Krot et al., 1998a) and an expected Curie temperature of 753 °C. Previous rock magnetic studies of Allende have not identified a magnetic phase with Curie temperature >610 °C, suggesting the complete removal of the primary low-Ni FeNi metal in Allende by alteration.

Alteration in Allende likely occurred on the CV parent body; veins of alteration minerals that crosscut chondrule–matrix boundaries strongly suggest post-accretional formation (Brearley, 1997; Kojima and Tomeoka, 1996; Krot et al., 1998a). Summarizing these lines of petrographic and rock magnetic evidence, all magnetic minerals in Allende likely formed during metasomatism on the CV parent body. No evidence exists for the survival of primary low-Ni FeNi phases from which the observed magnetic phases were altered.

CRM or TCRM due to recrystallization of magnetic phases in weak ambient fields may give rise to non-unidirectional magnetization at small scales. For example, CRM acquired in a <1 μT field is likely responsible for the non-unidirectional magnetization at the <5 mm scale carried by tetrataenite in the Bessou LL chondrite (Gattacceca et al., 2003).

Analogous to the HT magnetization in Allende and non-unidirectional magnetization in Bessou, randomly oriented magnetizations in the L6 chondrite ALH-769 that pass the paleomagnetic conglomerate test may also be due to post-accretional recrystallization instead of pre-accretional heating as previously argued (Funaki et al., 1981). In the case of ALH-769, the high metamorphic temperatures (>1000 °C; Bennett and McSweeney, 1996) preclude the retention of any pre-accretional magnetization.

Although in some cases secondary minerals may inherit the magnetization direction of its precursor mineral phases, such a process is usually important for reactions that do not involve a change in lattice structure (Dunlop and Özdemir, 1997). The formation of magnetite, pyrrhotite, and awaruite (fcc lattice) from 5% Ni metal (bcc lattice) in Allende would have led to rearrangement of the parent mineral structure, consistent with these minerals acquiring a spontaneous non-unidirectional CRM instead of inheriting pre-existing magnetization.

Given the pervasive alteration observed in Allende magnetic phases and the potential for recrystallization to result in non-unidirectional magnetization at the sub-chondrule scale, we conclude that CRM or TCRM acquired in a weak magnetic field during alteration is the most likely origin for the non-unidirectional HT magnetization observed in Allende chondrules. As such, although the HT magnetization passes the conglomerate test, Allende chondrules carry no discernible recording of ancient magnetic fields. We therefore do not refer to it as a magnetization “component”, in contrast to the unidirectional MT and LT components. Despite widespread practice, paleomagnetic results from Allende should not be used to constrain solar nebula magnetic fields or the chondrule-forming process. Future studies of pre-accretional magnetization in chondrules should conduct both the conglomerate test and the single chondrule unidirectionality test to establish the pre-accretional origin of magnetization.

4.2. Any dynamo on the CV parent body had declined before the end of metasomatism

The non-unidirectionality of the HT magnetization can constrain the strength of ambient magnetic fields during its acquisition. The background field strength must have been below the recording limit for a CRM/TCRM; otherwise, Allende samples would carry a unidirectional HT magnetization corresponding to the magnetic field during alteration (Fig. 8). The capacity for secondary minerals to acquire a CRM parallel to the direction of the ambient field depends on the specific alteration reaction (Dunlop and Özdemir, 1997). CRM acquisition during oxidation and sulfidation of low-Ni FeNi metal has not been experimentally studied. However, secondary formation of pyrrhotite and magnetite on Earth leads to recording of the ambient field direction (e.g., Dinarès-Turell and Dekkers, 1999; Haigh, 1958; Weaver et al., 2002). The strength of the ambient magnetic field during the acquisition of the HT magnetization was therefore likely significantly weaker than Earth-strength (i.e., $\ll 50 \mu\text{T}$). Furthermore, assuming that the efficiency of CRM acquisition is ~0.09 times that of an ARM (see SD for derivation), the 0.7 μT recording limit from our ARM acquisition experiments implies that the ambient field strength during the acquisition of the HT magnetization was likely <8 μT . We evaluate the implications of this constraint on the magnetic evolution of the CV parent body given two hypotheses for the origin of the MT overprint, which is found in class A chondrules and matrix material but is absent from class B chondrules.

4.2.1. Hypothesis I: the MT overprint is a partial TRM

Owing to its 290 °C maximum blocking temperature, which is distinct from the Curie points of ferromagnetic minerals in Allende, Carporzen et al. (2011) argued that the MT overprint is most likely a partial TRM acquired in a ~60 μT field (Fig. 8 top). Since class B chondrule samples are likely capable of recording a 290 °C partial TRM in magnetic fields stronger than ~2 μT (see Section 3.2), the absence of the MT overprint in class B chondrules requires a late remagnetization event that removed the previously recorded MT overprint but did not affect the overprint in class A chondrules and the matrix. No known heating mechanism can lead to the localized heating of only a subset of chondrules to >290 °C. Impact shock may lead to localized heating, but is expected to cause greater heating in the more porous matrix instead of chondrules (Muxworthy et al., 2011).

On the other hand, ongoing alteration or a late alteration event is capable of affecting a subset of chondrules while preserving the MT overprint in the adjacent material. As discussed above, such alteration in a <8 μT field may lead to the non-unidirectional NRM observed in class B chondrules. The early timing of metasomatism in the matrix and class A chondrules before the heating event that created the MT overprint would have led to the preservation of the MT magnetization (Fig. 8 top).

4.2.2. Hypothesis II: the MT overprint is a CRM or TCRM

Alternatively, we assume that the MT overprint is a CRM or TCRM (Nagata and Funaki, 1983) (Fig. 8 bottom). If class A chondrules and matrix material acquired the MT component in this fashion, then class B chondrules, which also contain secondary magnetic minerals (see Section 3.2 and Wasilewski and Saralker, 1981) should have acquired the same overprint if the alteration occurred concurrently. The metasomatism of magnetic phases in class B chondrules therefore must have taken place in a magnetic field weaker than both that of class A chondrules and matrix material and the CRM recording limit. I–Xe dating of the formation of secondary phases suggests that matrix material in Allende underwent alteration 0.5–3.2 My before chondrules (Swindle et al.,

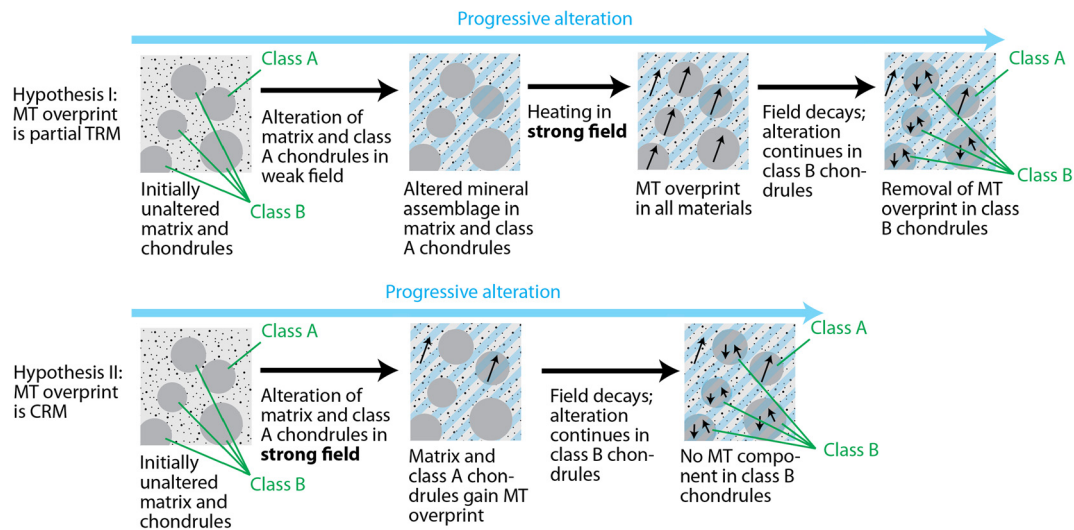


Fig. 8. Two possible alteration and magnetic histories for the Allende meteorite. Dark gray circles represent chondrules, speckled light gray surrounding represents matrix, and small black arrows represent magnetization. Light blue stripes denote chondrule and matrix materials that have undergone metasomatism, resulting in the recrystallization of all magnetic phases. (Top) Assuming that the MT overprint is a partial TRM (Carpurzen et al., 2011), a late alteration event is required to remove this overprint from class B chondrules. Because there is no unidirectional magnetization blocked to the Curie temperature, the first episode of metasomatism must have occurred in a near-zero field. Heating in a strong field (such as from a core dynamo) then imparted the MT component in all Allende materials. This MT magnetization was erased by late alteration in class B chondrules. This sequence of events can explain the presence of the MT component in class A chondrules but not in class B. (Bottom) Assuming that the MT overprint is a CRM or TCRM, the field could have been present from the beginning of alteration. Progressive alteration first altered the matrix and class A chondrules in the presence of a strong field (such as from a core dynamo), followed by alteration of class B chondrules in near-zero field. The field must have likewise decayed after the alteration of class A chondrules but before that of class B chondrules. (For interpretation of the references to color in this figure legend, the reader is referred to the web version of this article.)

1983). Therefore, if class A chondrules and matrix material acquired a CRM in the same strong field environment, this strong field epoch must have predated the weak field epoch during which alteration occurred in class B chondrules.

4.2.3. Synthesis

In the case of either a partial TRM or CRM/TCRM origin for the MT overprint, alteration in class B chondrules must have occurred later than in the matrix and class A chondrules in the absence of a $<8 \mu\text{T}$ magnetic field. In further support of these hypotheses, petrographic observations alteration minerals suggest that the matrix underwent the earliest alteration while chondrules were altered at a range of ages, with the cores of chondrules experiencing the least extensive and likely latest alteration (Brearley and Krot, 2012). Because in both cases alteration in class B chondrules occurred after the post-accretionary MT overprint, the setting of this alteration must have been on the CV parent body. Furthermore, the difference in the mineralogies of the dominant opaque phases (Fig. 5), which are all secondary in origin, for the two chondrule classes suggests that alteration in the two classes took place in distinct events or under progressively changing conditions.

Previous paleointensity estimates found that the unidirectional MT magnetization was likely acquired in an Earth-strength magnetic field ($\sim 60 \mu\text{T}$; Carpurzen et al., 2011). Due to the high paleointensity, unidirectionality, and inferred stability of this field, Carpurzen et al. (2011) concluded that it is most likely due to a core dynamo in the CV parent body. The low field environment in which class B chondrule material altered would correspond to after the cessation or decline of the dynamo. The alteration age of class B chondrule material would therefore provide an upper bound to the age of the purported magnetic core dynamo in the CV parent body.

Radiometric dating using the $^{129}\text{I}/^{129}\text{Xe}$ system may directly constrain the timing of alteration in Allende due to the high I content of sodalite, an abundant secondary mineral found in all Allende components (Kirschbaum, 1988). $^{129}\text{I}/^{129}\text{Xe}$ dates for individual Allende components suggest that sodalite formation contin-

ued during a span of up to ~ 10 My, with the latest major resetting occurring at 10–15 My after CAIs (Pravdivtseva et al., 2003; Swindle et al., 1988) when adopting an absolute age of 4562.3 Ma for Shallowater enstatite (Gilmour et al., 2009). Furthermore, limited alteration may have continued to cause Xe loss until up to 40 My after CAIs (Carpurzen et al., 2011). Based on the I–Xe data (see SD for discussion of other geochronological constraints), we propose that, assuming the ^{129}I carrier in Allende chondrules formed concurrently with the secondary magnetic phases, any core dynamo in the CV parent body had likely declined within 40 My of CAIs. This is broadly consistent with some theoretical models predicting a 10 to several 10s My lifetime for planetesimal dynamos (Elkins-Tanton et al., 2011; Sterenborg and Crowley, 2013).

5. Conclusion

We find that, after the removal of unidirectional, post-accretionary overprints blocked up to $\sim 290^\circ\text{C}$ (the LT and MT components), all Allende chondrules carry an HT magnetization. This magnetization is non-unidirectional across chondrules and subsamples of the same chondrule. Due to its stability over a range of blocking temperatures and its heterogeneity on <1 mm scales, we rule out a pre-accretionary TRM origin for the HT magnetization and conclude that it was most likely acquired during metasomatic replacement of primary magnetic phases in a low field ($<8 \mu\text{T}$) environment during alteration on the CV parent body. Allende chondrules therefore contain no discernable preaccretionary magnetization. Despite widespread practice, documented magnetization in Allende should not be used to constrain early protoplanetary disk fields and their possible roles in mass and angular momentum transfer, chondrules formation, and planetary accretion and migration (e.g., Levy and Araki, 1989; Stepinski, 1992; Rozyczka et al., 1996; Shu et al., 1996; Nübold and Glassmeier, 2000; Desch and Connolly, 2002; Johansen, 2009).

We found that all chondrule samples fall into one of two classes based on their remanent magnetization and rock magnetic properties. Class A chondrules, which make up $\sim 20\%$ of the sampled

chondrules, carry the MT overprint and exhibit random magnetization directions after demagnetization of this component at $\sim 290^\circ\text{C}$. Class B chondrules show non-unidirectional NRM and absence of the post-accretional MT overprint. Given that the magnetic minerals in Allende are of secondary origin and that alteration in Allende was a heterogeneous process spread across several My, late alteration in a weak field environment is the most plausible explanation for the lack of the MT overprint in class B chondrules. This scenario requires that any purported magnetic core dynamo had decayed before the end of alteration. Assuming that the I/Xe system records the last phases of magnetic mineral formation, then the lifetime of the CV parent body dynamo was ≤ 40 My.

Acknowledgements

We thank L. Carporzen and D.L. Shuster for discussions that improved the manuscript. We also thank Thomas F. Peterson and the NASA Origins program (NNX10AH32G) for support and D.S. Ebel and J. Boesenberg for providing the samples of Allende. Additional support for R.R. Fu was provided by the NSF Graduate Research Fellowship.

Appendix A. Supplementary material

Supplementary material related to this article can be found online at <http://dx.doi.org/10.1016/j.epsl.2014.07.014>.

References

- Acton, G., Yin, Q.Z., Verosub, K.L., Jovane, L., Roth, A., Jacobsen, B., Ebel, D.S., 2007. Micromagnetic coercivity distributions and interactions in chondrules with implications for paleointensities of the early solar system. *J. Geophys. Res.* 112. <http://dx.doi.org/10.1029/2006JB004655>.
- Bai, X.-N., Stone, J.M., 2013. Wind-driven accretion in protoplanetary disks. I. Suppression of the magnetorotational instability and launching of the magnetocentrifugal wind. *Astrophys. J.* 769.
- Balbus, S.A., 2003. Enhanced angular momentum transport in accretion disks. *Annu. Rev. Astron. Astrophys.* 41, 555–597.
- Baratchart, L., Hardin, D.P., Lima, E.A., Saff, E.B., Weiss, B.P., 2013. Characterizing kernels of operators related to thin-plate magnetizations via generalizations of Hodge decompositions. *Inverse Probl.* 29, 015004.
- Bennett, M.E., McSween, H.Y., 1996. Revised model calculations for the thermal histories of ordinary chondrite parent bodies. *Meteorit. Planet. Sci.* 31, 783–792.
- Brearely, A.J., 1997. Disordered biopyroxenes, amphibole, and talc in the Allende meteorite: products of nebular or parent body aqueous alteration? *Science* 276, 1103–1105.
- Brearely, A.J., Krot, A.N., 2012. Metasomatism in the early solar system: the record from chondritic meteorites. In: Harlow, D.E., Austrheim, H. (Eds.), *Metasomatism and the Chemical Transformation of Rock*. Springer-Verlag, Berlin, pp. 659–789.
- Butler, R.F., 1972. Natural remanent magnetization and thermomagnetic properties of Allende meteorite. *Earth Planet. Sci. Lett.* 17, 120–128.
- Carporzen, L., Weiss, B.P., Elkins-Tanton, L.T., Shuster, D.L., Ebel, D.S., Gattacceca, J., 2011. Magnetic evidence for a partially differentiated carbonaceous chondrite parent body. *Proc. Natl. Acad. Sci. USA* 108, 6386–6389.
- Chambers, J.E., 2004. Planetary accretion in the inner Solar System. *Earth Planet. Sci. Lett.* 223, 241–252.
- Choi, B.-G., McKeegan, K.D., Leshin, L.A., Wasson, J.T., 1997. Origin of magnetite in oxidized CV chondrites: in situ measurement of oxygen isotope compositions of Allende magnetite and olivine. *Earth Planet. Sci. Lett.* 146, 337–349.
- Cisowski, S.M., 1987. Magnetism of meteorites. In: Jacobs, J.A. (Ed.), *Geomagnetism*. Academic Press, London, pp. 525–560.
- Crutcher, R.M., 2012. Magnetic fields in molecular clouds. *Annu. Rev. Astron. Astrophys.* 50, 29–53.
- Cuzzi, J.N., Hogan, R.C., 2003. Blowing in the wind I. Velocities of chondrule-sized particles in a turbulent protoplanetary nebula. *Icarus* 164, 127–138.
- Desch, S.J., Connolly, H.C., 2002. A model of the thermal processing of particles in solar nebula shocks: application to the cooling rates of chondrules. *Meteorit. Planet. Sci.* 37, 183–207.
- Desch, S.J., Morris, M.A., Connolly, H.C., Boss, A.P., 2012. The importance of experiments: constraints on chondrule formation models. *Meteorit. Planet. Sci.* 47, 1139–1156.
- Dinarès-Turell, J., Dekkers, M.J., 1999. Diagenesis and remanence acquisition in the Lower Pliocene Trubi marls at Punta di Maiata (southern Sicily): palaeomagnetic and rock magnetic observations. In: Tarling, D.H., Turner, P. (Eds.), *Palaeomagnetism and Diagenesis in Sediments*. Geological Society, London, pp. 53–69.
- Dunlop, D.J., Özdemir, O., 1997. *Rock Magnetism: Fundamentals and Frontiers*. Cambridge University Press, New York.
- Elkins-Tanton, L.T., Weiss, B.P., Zuber, M.T., 2011. Chondrites as samples of differentiated planetesimals. *Earth Planet. Sci. Lett.* 305, 1–10.
- Emmerton, S., Muxworthy, A.R., Hezel, D.C., Bland, P.A., 2011. Magnetic characteristics of CV chondrules with paleointensity implications. *J. Geophys. Res.* 116, E12007.
- Fong, L.E., Holzer, J.R., McBride, K.K., Lima, E.A., Baudenbacher, F., 2005. High resolution room-temperature sample scanning superconducting interference device microscope configurable for geological and biomagnetic applications. *Rev. Sci. Instrum.* 76, 053703.
- Funaki, M., Nagata, T., Momose, K., 1981. Natural remanent magnetizations of chondrules, metallic grains and matrix of an Antarctic chondrite, ALH-769. *Mem. Natl. Inst. Polar Res. Spec. Issue* 20, 300–315.
- Funaki, M., Wasilewski, P., 1999. A relation of magnetization and sulfidization in the parent body of the Allende (CV3) carbonaceous meteorite. *Meteorit. Planet. Sci.* 34, A39.
- Gattacceca, J., Rochette, P., Bourot-Denise, M., 2003. Magnetic properties of a freshly fallen LL ordinary chondrite: the Bensour meteorite. *Phys. Earth Planet. Inter.* 140, 343–358.
- Gattacceca, J., Suavet, C., Rochette, P., Weiss, B.P., Winkhofer, M., Uehara, M., Friedrich, J.M., 2014. Metal phases in ordinary chondrites: magnetic hysteresis properties and implications for thermal history. *Meteorit. Planet. Sci.* 49, 652–676.
- Gilmour, J.D., Crowther, S.A., Busfield, A., Holland, G., Whitby, J.A., 2009. An early I–Xe age for CB chondrite chondrule formation, and a re-evaluation of the closure age of Shallowater enstatite. *Meteorit. Planet. Sci.* 44, 573–579.
- Haggerty, S.E., McMahon, B.M., 1979. Magnetite–sulfide–metal complexes in the Allende meteorite. In: *Proc. Lunar Planet. Sci. Conf.*, vol. 10, pp. 851–870.
- Haigh, G., 1958. The process of magnetization by chemical change. *Philos. Mag.* 3, 267–286.
- Johansen, A., 2009. The role of magnetic fields for planetary formation. In: Strassmeier, K.G., Kosovichev, A.G., Beckman, J.E. (Eds.), *Cosmic Magnetic Fields: From Planets, to Stars and Galaxies*. In: *Proc. IAU Symp.*, vol. 259, pp. 119–128.
- Johansen, A., Oishi, J.S., Mac Low, M.-M., Klahr, H., Henning, T., Youdin, A., 2007. Rapid planetesimal formation in turbulent circumstellar disks. *Nature* 448, 1022–1025.
- Kirschbaum, C., 1988. Carrier phases for iodine in the Allende meteorite and their associated Xe-129(R)/I-127 ratios – a laser microprobe study. *Geochim. Cosmochim. Acta* 52, 679–699.
- Kojima, T., Tomeoka, K., 1996. Indicators of aqueous alteration and thermal metamorphism on the CV parent body: microtextures of a dark inclusion from Allende. *Geochim. Cosmochim. Acta* 60, 2651–2666.
- Krot, A.N., Petaev, M.I., Scott, E.R.D., Choi, B.-G., Zolensky, M.E., Keil, K., 1998a. Progressive alteration in CV3 chondrites: more evidence for asteroidal alteration. *Meteorit. Planet. Sci.* 33, 1065–1085.
- Krot, A.N., Petaev, M.I., Zolensky, M., Keil, K., Scott, E.R.D., Nakamura, K., 1998b. Secondary calcium-iron-rich minerals in the Bali-like and Allende-like oxidized CV3 chondrites and Allende dark inclusions. *Meteorit. Planet. Sci.* 33, 623–645.
- Krot, A.N., Scott, E.R.D., Zolensky, M.E., 1997. Origin of fayalitic olivine rims and lath-shaped matrix olivine in the CV3 chondrite Allende and its dark inclusions. *Meteorit. Planet. Sci.* 32, 31–49.
- Lanoix, M., Strangway, D.W., Pearce, G.W., 1978. The primordial magnetic field preserved in chondrules of the Allende meteorite. *Geophys. Res. Lett.* 5, 73–76.
- Levy, E.H., Araki, S., 1989. Magnetic reconnection flares in the protoplanetary nebula and the possible origin of meteorite chondrules. *Icarus* 81, 74–91.
- Lima, E.A., Weiss, B.P., 2009. Obtaining vector magnetic field maps from single-component measurements of geological samples. *J. Geophys. Res.* 114, B06102. <http://dx.doi.org/10.1029/2008JB006006>.
- Lima, E.A., Weiss, B.P., Baratchart, L., Hardin, D.P., Saff, E.B., 2013. Fast inversion of magnetic field maps of unidirectional planar geological magnetization. *J. Geophys. Res.* 118, 2723–2752.
- MacPherson, G.J., 2007. Calcium-aluminum-rich inclusions in chondritic meteorites. In: *Treatise on Geochemistry*. Elsevier, pp. 1–47.
- McNally, C.P., Hubbard, A., Mac Low, M.-M., Ebel, D.S., D'Alessio, P., 2013. Mineral processing by short circuits in protoplanetary disks. *Astrophys. J.* 767, L2.
- McSween, H.Y., 1977. Petrographic variations among carbonaceous chondrites of the Vigarano type. *Geochim. Cosmochim. Acta* 41, 1777–1790.
- Muxworthy, A.R., Bland, P.A., Collins, G.S., Moore, J.M., Davison, T., Ciesla, F.J., 2011. Heterogeneous Shock in Porous Chondrites: Implications for Allende Magnetization. *AGU, San Francisco*, p. GP11B-07.
- Nagata, T., 1979a. Meteorite magnetism and the early solar system magnetic field. *Phys. Earth Planet. Inter.* 20, 324–341.
- Nagata, T., 1979b. Natural remanent magnetization of the fusion crust of meteorites. *Mem. Natl. Inst. Polar Res.* 15, 253–272.
- Nagata, T., Funaki, M., 1983. Paleointensity of the Allende carbonaceous chondrite. *Mem. Natl. Inst. Polar Res. Spec. Issue* 30, 403–434.

- Nübold, H., Glassmeier, K.-H., 2000. Accretional remanence of magnetized dust in the solar nebula. *Icarus* 144, 149–159.
- Pravdivtseva, O.V., Krot, A.N., Hohenberg, C.M., Meshik, A.P., Weisberg, M., Keil, K., 2003. The I–Xe record of alteration in the Allende CV chondrite. *Geochim. Cosmochim. Acta* 67, 5011–5026.
- Rozyczka, M., Bodenheimer, P., Lin, D.N.C., 1996. A numerical study of magnetic buoyancy in an accretion disk. *Astrophys. J.* 459, 371–383.
- Shu, F.H., Shang, H., Lee, T., 1996. Toward an astrophysical theory of chondrites. *Science* 271, 1545–1552.
- Stepinski, T.F., 1992. Generation of dynamo magnetic fields in the primordial solar nebula. *Icarus* 97, 130–141.
- Sterenberg, M.G., Crowley, J.W., 2013. Thermal evolution of early solar system planetesimals and the possibility of sustained dynamos. *Phys. Earth Planet. Inter.* 214, 53–73.
- Sugiura, N., Lanoix, M., Strangway, D.W., 1979. Magnetic fields of the solar nebula as recorded in chondrules from the Allende meteorite. *Phys. Earth Planet. Inter.* 20, 342–349.
- Sugiura, N., Matsui, T., Strangway, D.W., 1985. On the natural remanent magnetization in Allende meteorite. In: *Proc. Lunar Planet. Sci. Conf.*, vol. 16, pp. 831–832.
- Sugiura, N., Strangway, D.W., 1985. NRM directions around a centimeter-sized dark inclusion in Allende. In: *Proc. Lunar Planet. Sci. Conf.*, vol. 15, pp. C729–C738.
- Swartzendruber, L.J., Itkin, V.P., Alcock, C.B., 1991. The Fe–Ni (iron–nickel) system. *J. Phase Equilib.* 12, 288–312.
- Swindle, T.D., Caffee, M.W., Hohenberg, C.M., 1988. Iodine–xenon studies of Allende inclusions: Eggs and the Pink Angel. *Geochim. Cosmochim. Acta* 52, 2215–2227.
- Swindle, T.D., Caffee, M.W., Hohenberg, C.M., Lindstrom, M.M., 1983. I–Xe studies of individual Allende chondrules. *Geochim. Cosmochim. Acta* 47, 2157–2177.
- Tikoo, S.M., Weiss, B.P., Buz, J., Lima, E.A., Shea, E.K., Melo, G., Grove, T.L., 2012. Magnetic fidelity of lunar samples and implications for an ancient core dynamo. *Earth Planet. Sci. Lett.* 337–338, 93–103.
- Uehara, M., Gattacceca, J., Leroux, H., Jacob, D., van der Beek, C.J., 2011. Magnetic microstructures of metal grains in equilibrated ordinary chondrites and implications of paleomagnetism of meteorites. *Earth Planet. Sci. Lett.* 306, 241–252.
- Vaughan, D.J., Craig, J.R., 1978. *Mineral Chemistry of Metal Sulfides*. Cambridge University Press, Cambridge, UK.
- Wasilewski, P., 1981. New magnetic results from Allende C3(V). *Phys. Earth Planet. Inter.* 26, 134–148.
- Wasilewski, P.J., Saralker, C., 1981. Stable NRM and mineralogy in Allende: chondrules. In: *Proc. Lunar Planet. Sci. Conf.*, vol. 12, pp. 1217–1227.
- Watson, G.S., 1956. A test for randomness. *Mon. Not. R. Astron. Soc.* 7, 160–161.
- Weaver, R., Roberts, A.P., Barker, A.J., 2002. A late diagenetic (syn-folding) magnetization carried by pyrrhotite: implications for paleomagnetic studies from magnetic iron sulphide-bearing sediments. *Earth Planet. Sci. Lett.* 200, 371–386.
- Weisberg, M.K., McCoy, T.J., Krot, A.N., 2006. Systematics and evaluation of meteorite classification. In: Lauretta, D.S., McSween, H.Y. (Eds.), *Meteorites and the Early Solar System II*. University of Arizona, Tucson, pp. 19–52.
- Weiss, B.P., Gattacceca, J., Stanley, S., Rochette, P., Christensen, U.R., 2010. Paleomagnetic records of meteorites and early planetesimal differentiation. *Space Sci. Rev.* 152, 341–390.
- Weiss, B.P., Lima, E.A., Fong, L.E., Baudenbacher, F.J., 2007. Paleomagnetic analysis using SQUID microscopy. *J. Geophys. Res.* 112, B09105. <http://dx.doi.org/10.1029/2007JB004940>.

Supplementary Data

No nebular magnetization in the Allende CV carbonaceous chondrite

Roger R. Fu, Eduardo A. Lima, Benjamin P. Weiss

SQUID microscopy of isolated chondrules

To further confirm our finding that most Allende chondrules carry internally non-unidirectional magnetization, we mapped isolated chondrules using the SQUID Microscope. In comparison to SQUID microscopy of the Allende thin section (Section 3.1), these measurements avoid any possible effect on the field map from matrix material surrounding the chondrules.

We extracted the chondrules used for these experiments from the Allende slab AMNH4889, which has dimensions of $\sim 3.0 \times 3.5 \times 0.7$ cm and was also obtained from the American Museum of Natural History. This piece is not mutually oriented with respect to the AMNH5056 slab, although samples from within AMNH4889 are mutually oriented with respect to one another. To confirm the presence of extraterrestrial magnetization in AMNH4889, we perform a fusion crust baked contact test by extracting two fusion crust-bearing and two interior (>3 mm from fusion crust) samples. The angular separation of the NRM direction between the two samples in each set is $<14^\circ$ while the mean NRM of the fusion-crust subsamples is 42° away from that of the interior subsamples. The mean mass-normalized intensity of the interior samples' NRM is $1.5 \times 10^{-4} \text{ Am}^2\text{kg}^{-1}$, which agrees

closely with values for uncontaminated Allende bulk material [Table S1; Carporzen et al. (2011); Emmerton et al. (2011)]. AMNH4889 therefore passes the fusion crust baked contact test, strongly suggesting that its interior magnetization is extraterrestrial in origin.

We extracted five isolated chondrules from AMH4889. We cut a 0.4 mm thick section of AMNH4889 with a diamond wire saw and glued this section to a 150 μm thick quartz cover slip. Then using a degaussed, tungsten-carbide dental scribe mounted on an Electro Scientific Industries Inc. Micromill we extracted the chondrules by cutting through the chondrite section and the coverslip. Each extracted chondrule and quartz coverslip unit was mounted on a GE 124 quartz disk to be scanned on the SQUID Microscope. These isolated chondrules were measured at a sensor-to-sample distance of $\sim 200\text{ }\mu\text{m}$ with a step size of $50\text{ }\mu\text{m}$. Similar to the maps of the Allende thin section (see Section 2), these maps were bilinearly interpolated and downward continued to yield an effective sensor-to-sample distance of $100\text{ }\mu\text{m}$.

Magnetic field maps of these isolated chondrules (Fig. S1) further corroborate the non-unidirectional nature of Allende chondrule magnetization. The magnetic field $100\text{ }\mu\text{m}$ above the isolated chondrules show that each carries several non-unidirectionally oriented dipolar sources with similar magnitude. The heterogeneous nature of the interior magnetization in these samples and the large discrepancy between their best-fit NRM direction and that of bulk material suggest that they are class B chondrules (Fig. S1G). Sources are distributed throughout the interiors of the chondrules, which rules out contamination from residual matrix material as an origin of the magnetic signal.

We can also use the SQUID microscope maps of the Allende thin section (Fig. 6) to simulate the measurement of an isolated chondrule by applying a spatial window that

tapers off contributions to the magnetic field from outside of a single chondrule (see Section 3.2). Furthermore, unlike the unrestricted model employed in Section 3.2, we can restrict the magnetization sources to areas within the chondrule while solving for the magnetization distribution (Fig. 6G-H). As done previously in Section 3.2, we assume unidirectional magnetization and solve for the best-fit distribution of magnetic sources. We find large voids in the best-fit unidirectional model. As in the case of streaks in the unrestricted magnetization model (Fig. 6F), these voids are non-physical and are due to the inability of the unidirectional model to reproduce the strong observed negative (downward) fields (blue in Fig. 6E). At the locations where strong negative fields are measured, the magnetization distribution solution exhibits voids to increase the negative value by enhancing fringing fields from surrounding, positively magnetized regions (compare locations of negative fields in Fig. 6G with those of voids in Fig. 6H). These residuals are as large as the measured field at some locations and again well exceed our expected noise limit, indicating that the restricted unidirectional model cannot adequately reproduce the measured magnetic fields.

Recording limit experiments on Allende material

We performed two sets of ARM acquisition experiments on Allende materials to evaluate their capacity to acquire a pTRM or a CRM in a weak ambient field. First, as described in the main text, to constrain their capacity to record a pTRM, we find the recording limit of class B chondrules by imparting ARMs in low bias fields and observing the directional coherence of the resulting acquired magnetization. We used maximum AC fields of 290 mT and DC bias fields of 0.5, 0.7, 1.0, 2.0, 5.0, and 10.0 μ T in our ARM

acquisition experiments and fully demagnetized the sample using a 420 mT AF application between each ARM acquisition. We repeat the experiment five times for each sample and bias field and find the acquired ARM via vector subtraction of the sample moment before and after each ARM application. The direction of this acquired magnetization is then compared to the bias field direction. We performed one ARM acquisition experiment in a strong 100 μ T bias field for each sample to evaluate the degree of anisotropy. In each case, the 100 μ T ARM was within 2.5° of the bias field, justifying our direct comparison between the acquired ARMs and the bias field direction. Two out of three class B chondrules acquired a mean ARM consistent with the bias field direction at the 95% confidence level in a 2 μ T bias field while one chondrule successfully acquired a 1 μ T bias field ARM. No samples acquired a unidirectional magnetization in a 0.7 μ T bias field. Adopting a 0.7 μ T ARM recording limit and a 280°C partial TRM to ARM ratio ($pTRM/ARM$) of 0.373 (Carpözen et al., 2011), this class B chondrule would have recorded a unidirectional $pTRM$ overprint if cooled from 280°C in a >1.9 μ T field. Because this field is much weaker than the ~60 μ T paleointensity of the MT component, we conclude that at least some class B chondrules were capable of acquiring an MT component along with class A chondrule and matrix material during cooling from 280°, ruling out a high recording limit as an explanation for the absence of the MT overprint in class B chondrules.

Our ARM recording limit for class B chondrules constrains the ability for chondrules to record a CRM during late alteration on the CV parent body and therefore the magnetic field environment during that time. The true ratio between CRM and ARM intensity in a given bias field depends on the specific reaction producing the CRM (Dunlop and Özdemir, 1997). As noted in the main text, CRM acquisition during oxidation and sulfidation of low-

Ni metal has not been experimentally compared with ARM. Even so, we can approximate the intensity ratio between a CRM and an ARM using a simple identity:

$$\frac{CRM}{ARM} = \frac{CRM}{TRM} \frac{TRM}{pTRM} \frac{pTRM}{ARM} \quad (1)$$

where all three quantities on the right hand side have been experimental constrained. In general, the ratio between the intensity of a CRM and a *full* TRM (CRM/TRM) has an extreme range between 0.04 and 1 with typical values >0.1 (Gie and Biquand, 1988; Heider and Dunlop, 1987; Kobayashi, 1959; Stokking and Tauxe, 1990). Because ARM acquisition in Allende is directly calibrated to a 280°C pTRM instead of a full TRM, we must find in addition the ratio ($TRM/pTRM$). Thermal demagnetization of a near-saturation IRM in Allende chondrules shows that $40 \pm 10\%$ of the remanent magnetization is unblocked below 280°C (Fig. S3). The value of ($TRM/pTRM$) is therefore ~ 2.5 . This ratio would imply a full TRM to ARM ratio of approximately 1 given that the experimental $pTRM/ARM$ ratio of Allende material is 0.373 (Carpornzen et al., 2011). A TRM to ARM ratio of ~ 1 is broadly consistent with most meteoritic samples (Lappe et al., 2013; Morden, 1992), thereby corroborating the accuracy of this value. Adopting the full range of possible values for the CRM/TRM , we find that CRM/ARM is between 0.036 and 0.93 with a likely value of >0.093 . A 0.7 μT ARM is therefore likely to have a similar intensity as an 8 μT CRM. Given that there may be greater noise during ARM acquisition compared to that of a TRM or a CRM, the recording limit of a CRM may be $<8 \mu T$. In any case, our recording limit experiments imply that the ambient field strength during late alteration of class B chondrules was $<8 \mu T$. This paleointensity is much lower than that of the MT component ($\sim 60 \mu T$), implying the decay if not the cessation of any dynamo on the CV parent body.

Second, we impart an ARM on one class A chondrule, four class B chondrules, and one matrix-rich sample in a 15 μT bias to simulate TRM acquisition in a ~ 40 μT bias field, which is reasonable lower bound for the MT component paleointensity (Carpenter et al., 2011). All chondrule and matrix samples acquired a strong, unidirectional [4×10^{-5} – 2×10^{-4} $\text{Am}^2\text{kg}^{-1}$; $P < 0.001$ (Watson, 1956)] ARM oriented $< 6^\circ$ from the bias field direction. This range of magnetization intensities is consistent with the observed strength of the MT component in class A chondrules samples and matrix samples. We conclude that both class A and B chondrules and matrix-rich samples are capable of recording a TRM or partial TRM during cooling in a field of ~ 40 μT . The lack of the MT component in class B chondrules is therefore not due to their inability to record such a field as a TRM.

Finally, we perform thermal demagnetization of a near-saturation IRM acquired in a 0.9 T field on one class A chondrule, three class B chondrules, and one matrix-rich sample. We find that approximately 30% of the IRM in class B chondrules unblocked between room temperature and 280°C (Fig. S3), implying that the absence of the MT component in class B chondrules cannot be attributed to their lack of magnetic carriers in the appropriate blocking temperature range. Consistent with the greater abundance of magnetic sulfides in class A chondrules and the matrix (see Main Text Section 3.2 and Fig. 5), the class A chondrule and matrix-rich samples showed greater demagnetization below 280°C (50% and 80% of initial magnetization, respectively).

Modeling of TRM acquisition in the solar nebula

We model the cooling history of chondrules required for the HT magnetization to be a pre-accretion TRM as suggested by previous studies. Because the HT magnetization is

non-unidirectional within single chondrules and is directionally stable between $\sim 100^{\circ}\text{C}$ (in class B chondrules) and $>420^{\circ}\text{C}$, a TRM origin would require that a sector of a single chondrule was heated to $>420^{\circ}\text{C}$ and cooled in the presence of a stable magnetic field without affecting the magnetization of adjacent sections of the same chondrule. Assuming a basalt-like thermal diffusivity of $6 \times 10^{-7} \text{ m}^2\text{s}^{-1}$ (Hanley et al., 1978), the timescale of thermal diffusion across a 1 mm chondrule is $\sim 2 \text{ s}$. Non-unidirectional TRM acquisition within a single chondrule therefore requires that one sector of a chondrule cooled from $>420^{\circ}\text{C}$ to 100°C within this timeframe; otherwise, adjacent sectors of the chondrule would have acquired a partial TRM in the same direction, leading to unidirectional magnetization among chondrule subsamples for at least a part of the blocking temperature range.

We therefore estimate the cooling rate of a hemisphere of a radius $r = 0.5 \text{ mm}$ diameter chondrule heated to 400°C . Assuming purely radiative heat transfer, the rate of heat loss in the heated hemisphere can be estimated from the Stefan-Boltzmann law:

$$\frac{dE}{dt} = -A\sigma T^4(t) \quad (2)$$

where dE/dt is the rate of thermal energy loss, $A = 2\pi r^2$ is the exposed surface area, σ is the Stefan-Boltzmann constant, and T is the temperature in Kelvin. Substituting the surface area for a hemisphere and $dE = c_p m dT$ where c_p is the specific heat capacity and m is the hemisphere's mass, we arrive at the differential equation:

$$\frac{dT}{dt} = -\frac{3\sigma}{c_p \rho r} T^4 \quad (3)$$

where ρ is the density assumed to be 3.66 g cm^{-3} , and c_p is $900 \text{ J kg}^{-1} \text{ K}^{-1}$ (Hughes, 1980; Vosteen and Schellschmidt, 2003). This differential equation yields the solution:

$$T(t) = \frac{1}{\left(\frac{9\sigma}{c_p \rho r} t + T_0^{-3} \right)^{1/3}} \quad (4)$$

where T_0 is the temperature at $t=0$. Substituting $T_0=693 \text{ K}$, we find that a chondrule hemisphere initially at 420°C cools by only $\sim 15^\circ\text{C}$ during the first 2 seconds. A chondrule in the presence of heated nebular gas (Desch and Connolly, 2002; McNally et al., 2013) would experience even slower cooling. The cooling timescale of a chondrule section is therefore much longer than the timescale needed to thermally equilibrate all sections of the chondrule. Therefore, TRM acquired in the solar nebula cannot account for the internally non-unidirectional HT magnetization observed in Allende chondrules.

Radiometric constraints on the age of Allende alteration

The absence of the MT component magnetization in class B chondrules, combined with the secondary nature of all Allende ferromagnetic phases, suggests that any purported dynamo on the CV parent body had decayed before the end of chondrule alteration (Section 4). Therefore, the age of alteration in Allende chondrules would provide an upper bound for the duration of the core dynamo.

Data from several radioisotope systems have been interpreted to constrain the timing of secondary alteration on the CV parent body. Although no radiometric ages directly date the formation of ferromagnetic phases, in the main text we cited the I/Xe system as the most likely to constrain the age of magnetic carrier. The primary carrier phase of I in Allende is sodalite (Kirschbaum, 1988), which, like magnetite and pentlandite, occurs only in the most highly altered CV chondrites. This correspondence in occurrence suggests that these minerals formed in the same metasomatic event (Krot et al., 1998a). We adopt ~40 My after CAIs as the age for the latest disturbance to the I/Xe system (Carporzen et al., 2011), implying that the dynamo on the CV parent body had decayed before this time.

Beside the I/Xe system, the $^{87}\text{Rb}/^{87}\text{Sr}$ age of Allende chondrules may suggest mobilization of Rb at 4.36 ± 0.08 Ga, nearly 200 My after the assembly of the CV parent body (Shimoda et al., 2005). However, late disturbance to the Rb/Sr system in Allende chondrule likely occurred only in the mesostasis (Shimoda et al., 2005), in which elements are more vulnerable to aqueous remobilization compared to in crystalline carriers such as nepheline or sodalite (Kojima and Tomeoka, 1996). Therefore, the 4.36 ± 0.08 Ga isochron from the Rb/Sr system is unlikely to constrain the original crystallization age of secondary Allende phases. At even younger ages, the $^{187}\text{Re}/^{187}\text{Os}$ system has been disturbed at 1.6 Ga (Archer et al., 2014) while radiogenic Pb may have been remobilized at ~100 Ma (Tatsumoto et al., 1976). However, both late ages likely reflect the fluid-assisted redistribution of Re/Os and Pb, respectively. No other radioisotope system shows disturbances at these ages, which would be expected if these ages correspond to a significant secondary recrystallization event. Moreover, uncertainty about the host phases

of Re and U implies that these young ages cannot be confidently interpreted as the crystallization age of any secondary mineral.

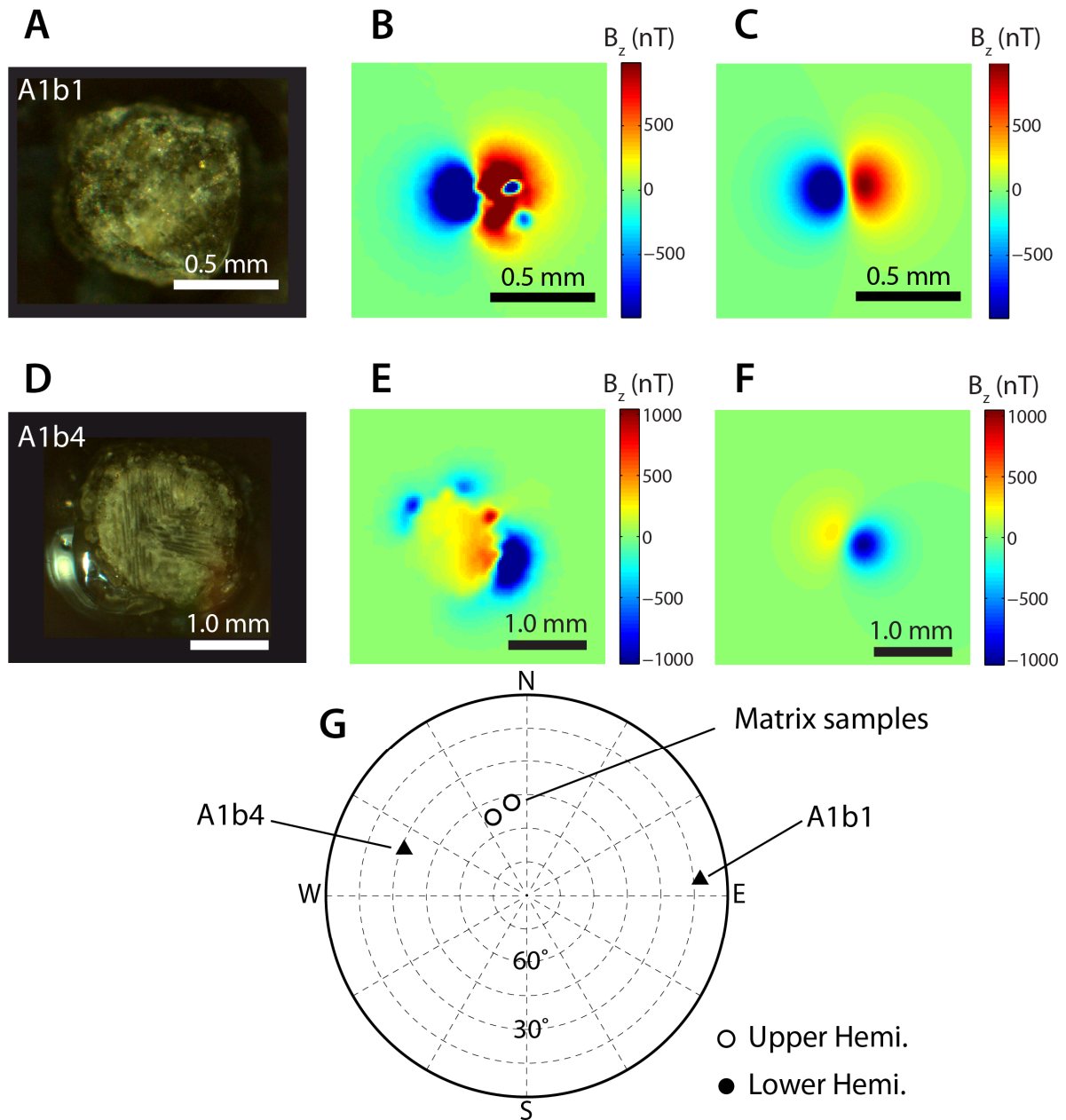


Fig. S1. SQUID Microscope analyses of two isolated Allende chondrules (samples A1b1 and A1b4). Shown are reflected light, crossed polars photomicrographs (A, D), measured vertical magnetic field maps (B, E), and model vertical fields from best-fit unidirectional, dipolar sources (C, F). Magnetic fields were mapped 200 μm above the chondrules and downward continued to 100 μm . Fields maps of both chondrules indicate multiple, non-unidirectional dipolar sources that are similar in strength. Best-fit model maps are calculated using single dipolar sources magnetized in the direction that minimizes the residual between the observed and modeled vertical magnetic field. (G) Equal area stereographic projections of the NRM directions of two matrix-rich samples and the best-fit NRM directions of the two isolated chondrules (note that these matrix directions differ from those plotted in Figs. 1 and 2 because these samples were extracted from the AMNH4889 piece, which is not mutually oriented with respect to the AMNH5059 piece; see Section 2). Due to the large difference before their best-fit NRM direction and that of the matrix, both isolated chondrules are of class B.

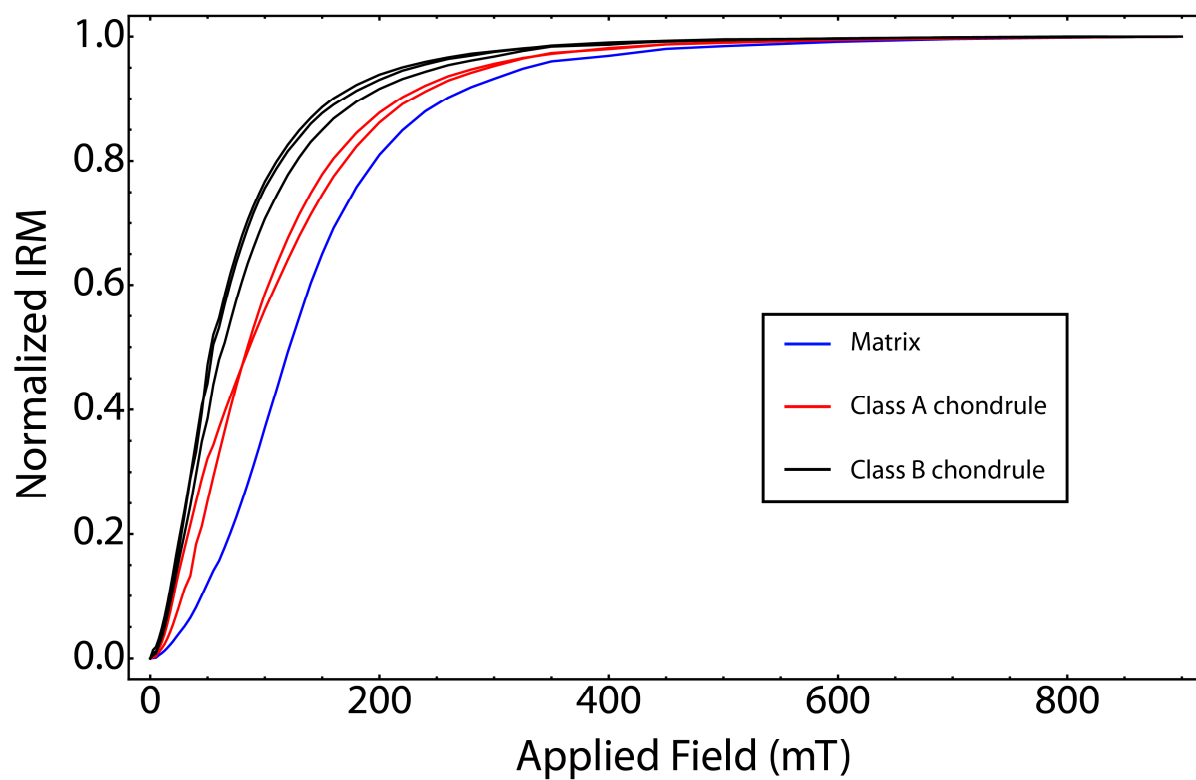


Fig. S2. Saturation IRM acquisition of class A chondrules, class B chondrules, and a matrix sample. The class A chondrules shown here are H28 and H29, the class B chondrules are H8, H18, and H22, and the matrix sample is MD.

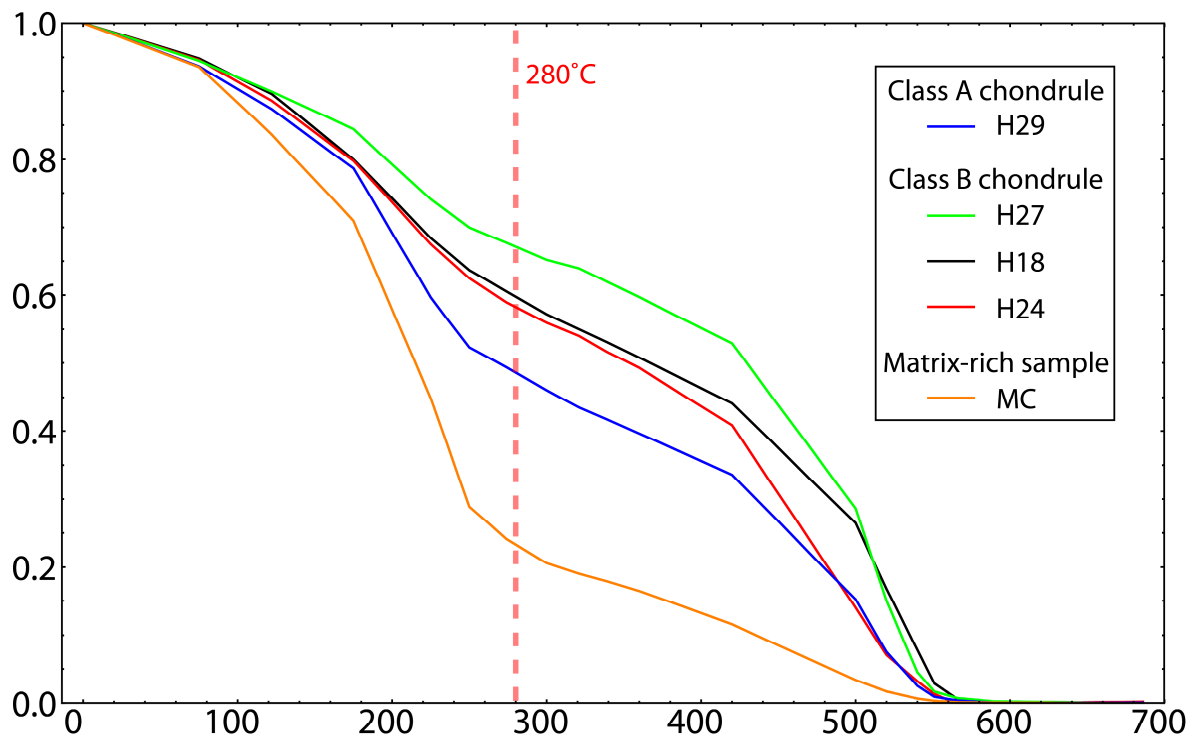


Fig. S3. Stepwise thermal demagnetization of a near-saturation 0.9 T IRM. The rapid decay of magnetization in the matrix-rich sample below the 280°C unblocking temperature of the MT component suggests that pyrrhotite is the dominant magnetic carrier. Approximately 40% of remanent magnetization in chondrules also unblocks below 280°C, implying that all should have recorded the MT overprint if cooled in a field from this temperature. Based on petrographic data (see Section 3.2), the loss of magnetization near 560°C likely represents a mixture of magnetite and awaruite.

Table S1: Summary of matrix samples. RT stands for "room temperature."

Thermal Demagnetization							
Sample name	Mass (mg)	NRM (Am ² kg ⁻¹)	Component	Thermal range	Dec, Inc (°)	MAD	N _m
MB	5.4	2.59×10 ⁻⁴	LT	RT-100°C	92.5, 26.0	8.4	3
			MT	110-280°C	57.7, 23.7	9.6	4
ME	3.7	1.95×10 ⁻⁴	LT	RT-125°C	87.7, 27.6	7.6	3
			MT	125-250°C	59.9, 24.0	3.9	4
			HT	250-325°C	85.0, 55.1	8.6	5
MF	3.4	1.95×10 ⁻⁴	LT	RT-285°C	72.2, 25.1	3.6	6
MG	5.1	2.10×10 ⁻⁴	LT	RT-127°C	98.3, 30.0	3.5	3
			MT	127-286°C	52.8, 30.3	2.9	9
			HT	286-450°C	157.2, 3.5	11.3	7
AF Demagnetization							
Sample name	Mass (mg)	NRM (Am ² kg ⁻¹)	Component	AF range	Dec, Inc (°)	MAD	N _m
MD	3.7	1.90×10 ⁻⁴	HC	0->85 mT	71.7, 21.6	10.1	109
MH	1.3	1.95×10 ⁻⁴	HC	0->85 mT	84.0, 38.7	20.4	109

Sample name	Mass (mg)	Class	NRM ($\text{Am}^2 \text{ kg}^{-1}$)
H6a	3.8	B	1.6×10^{-5}
H6b	2.7	B	1.1×10^{-6}
H24	2.7	B	2.4×10^{-5}
H27	2.7	B	2.3×10^{-5}
H32	2.5	B	5.9×10^{-5}

References

- Archer, G.J., Ash, R.D., Bullock, E.S., Walker, R.J., 2014. Highly siderophile elements and ^{187}Re – ^{187}Os isotopic systematics of the Allende meteorite: evidence for primary nebular processes and late-stage alteration. *Geochim. Cosmochim. Acta* 131, 402–414.
- Gie, T.I., Biquand, D., 1988. Etude experimentale de l'aimantation remanente chimique acquise au cours des tranformations reciproques hematite–magnetite. *J. Geomagn. Geoelectr.* 40, 177–206.
- Hanley, E.J., Dewitt, D.P., Roy, R.F., 1978. The thermal diffusivity of eight well-characterized rocks for the temperature range 300–1000 K. *Eng. Geol.* 12, 31–47.
- Heider, F., Dunlop, D.J., 1987. Two types of chemical remanent magnetization during the oxidation of magnetite. *Phys. Earth Planet. Inter.* 46, 24–45.
- Hughes, D.W., 1980. The dependence of chondrule density on chondrule size. *Earth Planet. Sci. Lett.* 51, 26–28.
- Kobayashi, K., 1959. Chemical remanent magnetization of ferromagnetic minerals and its application to rock magnetism. *J. Geomagn. Geoelectr.* 10, 99–117.
- Lappe, S.-C.L.L., Harrison, R.J., Feinberg, J.M., Muxworthy, A., 2013. Comparison and calibration of nonheating paleointensity methods: a case study using dusty olivine. *Geochem. Geophys. Geosyst.* 14, 1–16.
- Morden, S.J., 1992. A magnetic study of the Millbillillie (eucrite) achondrite: evidence for dynamo-type magnetising field. *Meteoritics* 27, 560–567.
- Shimoda, G., Nakamura, N., Kimura, M., Kani, T., Nohda, S., Yamamoto, K., 2005. Evidence from the Rb–Sr system for 4.4 Ga alteration of chondrules in the Allende (CV3) parent body. *Meteorit. Planet. Sci.* 40, 1059–1072.
- Stokking, L.B., Tauxe, L., 1990. Properties of chemical remanence in synthetic hematite: testing theoretical predictions. *J. Geophys. Res.* 95, 12639–12652.
- Tatsumoto, M., Unruh, D.M., Desborough, G.A., 1976. U–Th–Pb and Rb–Sr systematics of Allende and the U–Th–Pb systematics of Orgueil. *Geochim. Cosmochim. Acta* 40, 617–634.
- Vosteen, H.-D., Schellschmidt, R., 2003. Influence of temperature on thermal conductivity, thermal capacity and thermal diffusivity for different types of rock. *Phys. Chem. Earth* 28, 499–509.